Millennial-scale changes in abundance of brachiopods in bathyal environments detected by postmortem age distributions in death assemblage (Bari Canyon, Adriatic Sea)

Adam Tomašových[1]*, Diego A. García-Ramos[2], Rafał Nawrot[3], James H. Nebelsick[4] and Martin Zuschin[3]

[1]Earth Science Institute, Slovak Academy of Sciences, Bratislava 84005, Slovakia

[2]Università degli Studi di Ferrara, Dipartamento di Fisica e Scienze della Terra, Via Saragat 1, 44122 Ferrara, Italy

[3]Department of Palaeontology, University of Vienna, Althanstrasse 14, 1090 Vienna, Austria

[4]Department of Geosciences, University of Tübingen, Schnarrenbergstrasse 94-96, 72076 Tübingen, Germany

Present addresses: DAGR, Geological Survey of Austria, Neulinggasse, 38, A-1030 Vienna, Austria

AT, 0000-0002-0471-9480

*Correspondence: adam.tomasovych@savba.sk

Abstract: Inferring the composition of pre-Anthropocene baseline communities on the basis of death assemblages (DAs) preserved in a surface mixed layer requires discriminating among recently-dead shells sourced by living populations and older shells from extirpated populations. Here, we assess the distribution of postmortem ages in the DA formed by the brachiopod *Gryphus vitreus* at 580 m depth in the Bari Canyon (Adriatic Sea), with no individuals collected alive. The *Gryphus* DA exhibits millennial time averaging (inter-quartile range = 1250 years) and two modes in abundance at 500 and 1750 years BP. As high abundance of species in time-averaged DAs can reflect passive accumulation of shells sourced by populations with low standing population density, we reconstruct changes in annual density on the basis of the abundance maxima detected in the distribution of postmortem ages and on the basis of estimates of per-specimen disintegration rate. We find that adults (>20 mm) achieved densities of at least 10–20 individuals/m^2 (assuming lifespan is 10 years), and the pulses in abundance were thus associated with a high population density in the past, followed by the decline over the last few centuries. We infer that bathyal populations were volatile during the Late Holocene, with brachiopods sensitive to siltation that was induced by temporal changes in sediment dispersal into the Bari Canyon due to deforestation and climatic changes.

Supplementary material: Age data and R language scripts that replicate analyses are available at https://doi.org/10.6084/m9.figshare.c.6228410

Bathyal environments are increasingly affected by anthropogenic impacts induced by trawling (Rogers 1999; Roberts *et al.* 2000; Edinger and Sherwood 2012), litter in submarine canyons incising narrow shelves (Fabri *et al.* 2014; Fernandez-Arcaya *et al.* 2017), acidification (Turley *et al.* 2007; Ramirez-Llodra *et al.* 2011; Maier *et al.* 2012, 2013; Georgian *et al.* 2016; Baco *et al.* 2017), and by changes in seawater temperature and in the strength of the biological carbon pump (Morato *et al.* 2020; Chaikin *et al.* 2022). Understanding the volatility and resilience of bathyal ecosystems to such disturbances requires the assessment of their long-term dynamics during the Pleistocene and Holocene (Yasuhara *et al.* 2008; Thiagarajan *et al.* 2013). Sediment cores can be used to extract ecosystem history from fossil assemblages (e.g. Moffitt *et al.* 2015). However, bathyal environments are characterized by slow sedimentation or complex sedimentation affected by condensation, redeposition and episodic burial (Middelburg *et al.* 1997; Tyson 2001). In such settings, skeletal remains accumulating over multiple millennia are mixed within the upper decimetres of seabeds where they are actively affected by taphonomic processes. Such surface death assemblages (DAs) thus do not have sufficient stratigraphic resolution to discriminate ecological history at decadal or centennial resolution. However, they still (1) provide information on time-averaged composition of baseline communities (Kidwell 2007; Jonkers *et al.* 2019; Rillo *et al.* 2019) and (2) if coupled with dating of individual shells,

From: Nawrot, R., Dominici, S., Tomašových, A. and Zuschin, M. (eds) *Conservation Palaeobiology of Marine Ecosystems*. Geological Society, London, Special Publications, **529**,
https://doi.org/10.1144/SP529-2022-117

they can be used to restore fine-scale temporal resolution and track fluctuations in abundance of shell producers in the past at decadal (Albano *et al.* 2016), centennial (Tomašových *et al.* 2017), millennial (Carroll *et al.* 2003; Krause *et al.* 2010; Perry and Smithers 2011; Dexter *et al.* 2014; Tomašových *et al.* 2016), or multi-millennial scales (Thiagarajan *et al.* 2013; Margolin *et al.* 2014). Age dating of species that occur at high abundance in DAs, especially when shell producers are missing in living assemblages (LAs) collected in the same area, can detect whether the lack of living individuals of such species reflects (1) short-term, annual variability in abundance (Albano *et al.* 2016), (2) an unprecedented decline in production during the recent decades or centuries (potential signature of anthropogenic impacts, Kowalewski *et al.* 2000; Simões *et al.* 2009; Tomašových *et al.* 2019), (3) long-term variability driven by millennial-scale climatic changes unrelated to anthropogenic impacts (Ritter *et al.* 2017; Pratt *et al.* 2019; Vertino *et al.* 2019), or (4) other sources of mismatch related to transport, reworking, and differences in species preservation rates (e.g. Dominici and Zuschin 2005; Kidwell 2008).

Frequency distributions of postmortem ages of shells in DAs collected in the uppermost centimetres of a seabed are expected to be exponential or heavy-tailed rather than flat under steady input of shells as they are subjected to burial and disintegration in the taphonomic active zone (TAZ, Davies *et al.* 1989; Flessa *et al.* 1993; Olszewski 1999, 2004; Kosnik *et al.* 2013; Albano *et al.* 2020; Agiadi *et al.* 2022). However, internal modes or significant gaps in abundance of cohorts within such distributions of postmortem ages are diagnostic of significant fluctuations in abundance of populations over the duration of time averaging (Krause *et al.* 2010; Tomašových *et al.* 2016; Vertino *et al.* 2019). Although high time averaging of shells within a single stratigraphic increment or in a seabed averages out high-frequency fluctuations in assemblage composition and thus complicates palaeoecological inferences about short-term dynamics, age distributions of time-averaged populations reverse the loss of high-resolution information. When burial and disintegration rates of shells and lifespans of their producers can be approximated, the species abundances in time-averaged DAs can be unmixed and scaled down to the yearly ecological density (Kowalewski *et al.* 2000; Tomašových and Kidwell 2017), thus overcoming the gap between the nature of ecological and palaeoecological abundance data. For example, the distributions of postmortem shell ages can be used to detect whether dead-only species had very low standing densities at yearly scales and just accrued their high abundance in DAs in the course of extended time averaging or whether they achieved high annual standing densities (Tomašových *et al.* 2017).

When sedimentation rates are very low, age distributions of shells in a surface mixed layer can track fluctuations over relatively long (millennial) time-scales *if* shell disintegration rates in the mixed layer are slow (either within the TAZ or within protected microenvironments when the TAZ is patchy), because fast disintegration (1) prohibits preservation of old cohorts in the TAZ close to the sediment–water interface, and (2) pulls the postmortem age of modal classes towards the Recent (Tomašových *et al.* 2016). With increasing disintegration rate in the mixed layer, age structure of surface DAs thus increasingly deviates from the original time series in abundance (Tomašových *et al.* 2016). Very slow disintegration can lead to almost uniform distributions of postmortem ages under steady input of shells, but such conditions are unusual in present-day shelf environments with intense recycling of organic matter inducing carbonate deterioration (Walter *et al.* 1993), leading to strongly right-skewed age distributions in surface DAs (Kidwell *et al.* 2005; Kosnik *et al.* 2007, 2009; Tomašových *et al.* 2014; Olszewski and Kaufman 2015).

DAs, however, with very old, early Holocene or late Pleistocene aragonitic skeletal remains, stained by ferromanganese coatings and carrying diverse early-diagenetic signatures, frequently occur in mixed-bottom sediments or on firm- or hardgrounds in bathyal environments (Noé *et al.* 2006; Freiwald *et al.* 2009; Angeletti and Taviani 2011; Angeletti *et al.* 2015), indicating that the disintegration rate of skeletal remains in the mixed layer is slow in these settings. For instance, cold-water corals in the Mediterranean Sea (with unusually warm and saturated conditions relative to other deep-sea environments), but also in the NE Atlantic Ocean, are frequently preserved in surface DAs not associated with living populations. Their radiocarbon ages indicate distributional shifts and significant fluctuations in their abundance on the transition to the Holocene (Delibrias and Taviani 1984; Schröder-Ritzrau *et al.* 2005; Vertino *et al.* 2019).

Here, we focus on the frequency distribution of postmortem ages of a surface DA formed by the epifaunal brachiopod *Gryphus vitreus* in the middle bathyal (580 m) mixed-bottom habitats in the Bari Canyon of the Southern Adriatic Sea (Figs 1 & 2). This species presently forms dense aggregations with more than 10–100 living individuals/m^2 in the Western Mediterranean Sea (Emig 1985, 1989*a*; Cartes *et al.* 2009). Such densities of living populations have not been observed in the Eastern Mediterranean Sea. We identify the timing of past fluctuations in abundance of the brachiopod *Gryphus vitreus* in the southern Adriatic Sea and discuss how the effect of disintegration modifies the shape of frequency

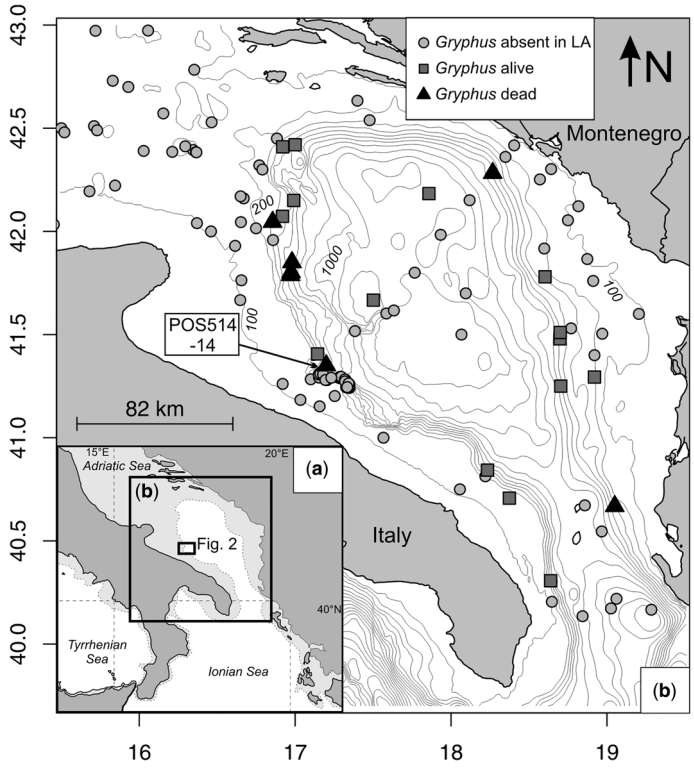

Fig. 1. (**a**) Geographical map of the southern Adriatic Sea with the location of the Bari Canyon, with light-grey colours corresponding to shelf segments, and the insets showing the positions of (b) and Figure 2. (**b**) Geographical distribution of stations in the southern Adriatic Sea with (dark grey squares) and without (light grey circles) *Gryphus vitreus* collected alive, and samples with dead-only collected *G. vitreus* (black triangles). The station POS514-14 in the Bari Canyon is investigated in this study. In total, 10% of all sites compiled on the basis of these published data (15 out of 130 sites in total, at water depths >100 m) contained individuals of this species collected alive in the Southern Adriatic Pit. These occurrences are based on samples collected during the Pola expedition in 1894 (Sturany 1896), grabs and trawls in 1969–70 documented by Gamulin-Brida (1983) off the Montenegrin coast, trawls documented by Marano *et al.* (1989), trawling survey PIPETA 1 in 1982 (Šimunović 1997), grab samples collected by the Poseidon cruise in 2017 (POS514), and samples documented in d'Onghia *et al.* (2015). The coordinates of death assemblages with *G. vitreus* are based on Trincardi *et al.* (2011) and on two stations collected by Poseidon in 2017. LA, living assemblage.

distributions of postmortem ages in DAs relative to the original chronological changes in abundances.

Gryphus vitreus

Gryphus vitreus is a suspension-feeding brachiopod with a smooth, punctate shell, attached to rocks, gravel or skeletal debris with a pedicle (Fig. 3). It can become secondarily free-lying when its substrate degrades or collapses (Emig 1987). It reaches 20–40 mm length in the adult stage (Boullier *et al.* 1986), and possesses a cyrtomatodont hinge (characterized by interlocked teeth and sockets) that prevents disarticulation to some degree. In contrast to most rhynchonelliformean brachiopods with two shell layers represented by the outer, very thin cryptocrystalline primary layer and the inner, thicker secondary layer consisting of fibres, *G. vitreus* possesses also a third, innermost prismatic tertiary layer that is mainly developed in the posterior and central segments of the valves (Gaspard 1989, 2011; Emig 1990; Gaspard *et al.* 2007; von Allmen *et al.* 2010; Romanin *et al.* 2018).

Gryphus vitreus is abundant in level-bottom benthic communities inhabiting detritic, mixed-bottom, shelf-edge or bathyal habitats of the Mediterranean Sea. In the Western Mediterranean Sea, this species occurs between 110 and 250 m at Corsica and Provence (Emig 1985, 1987, 1989*a*), between 110 and 330 m in the Menorca Channel (Grinyó *et al.* 2018), and between 600 and 2200 m in the

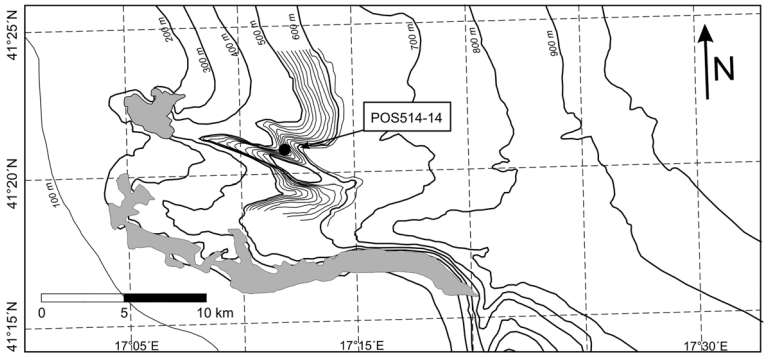

Fig. 2. The location of the sampling station POS514-14 (black circle) on the northern edge of the northern channel of the Bari Canyon in the southern Adriatic Sea (modified according to Trincardi *et al.* 2007*a*, *b*; Angeletti *et al.* 2020). The grey-shaded areas mark the location of epibenthic communities with corals, sponges and serpulids as mapped by Angeletti *et al.* (2020).

Balearic Sea (Cartes *et al.* 2009). In the Eastern Mediterranean Sea, live *G. vitreus* was reported from 497 to 790 m in the Santa Maria di Leuca deep-water cold-coral mound province in the Ionian Sea (Mastrototaro *et al.* 2010; Rosso *et al.* 2010), and is also known to occur in the Aegean and Levantine seas (Brunton 1988; Logan *et al.* 2002; Gönülal and Güresen 2014). Former dredging and trawling surveys in the southern Adriatic Sea documented several occurrences of live-collected *G. vitreus* at bathyal depths between 300 and 1140 m in the nineteenth century (Sturany 1896) and in the twentieth century (Gamulin-Brida 1983; Marano *et al.* 1989; Šimunović 1997; Fig. 1). However, several more recent surveys did not detect this species alive (Angeletti *et al.* 2014, 2020; D'Onghia *et al.* 2015).

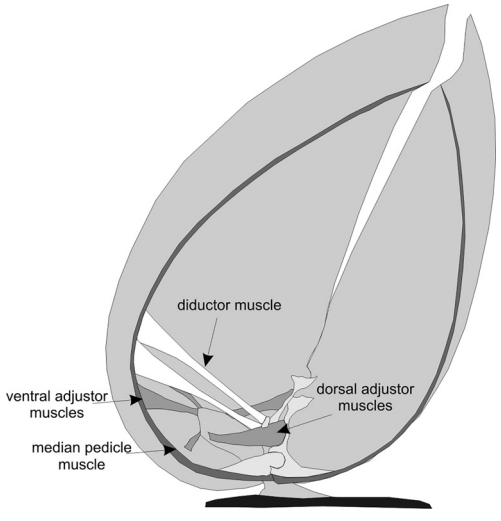

Fig. 3. Life position of *Gryphus vitreus* attached with the pedicle to a hard substrate (shell, gravel) in the adult stage (*c.* 3 cm in length), with dorsal and ventral adjustor muscles that can rotate and tilt shells with respect to its substrate. Source: adapted from Cox (1934) and Delance and Emig (2004)

Study area

Sedimentation in the SW Adriatic Sea is affected by thermohaline bottom currents of the North Adriatic Dense Water (NADW) that advect sediment and organic detritus downslope and interact with a complex topography of the Bari Canyon, leading to a mosaic of non-depositional and depositional conditions (Trincardi *et al.* 2007*a*, *b*; Verdicchio *et al.* 2007; Ridente *et al.* 2007). The high fluxes of suspended food particles delivered by the cascading currents of the NADW in the Bari Canyon System also support epibenthic communities (Turchetto *et al.* 2007; Tesi *et al.* 2008; Bo *et al.* 2012; Foglini *et al.* 2016). The slopes and flanks of the Bari Canyon are inhabited by cold-water colonial and solitary corals that form three-dimensional structures (up to 80 cm high) at 305–650 m (Taviani *et al.* 2016), dominated by *Madrepora oculata* (280–550 m, d'Onghia *et al.* 2015), frequently in association with serpulids (Sanfilippo *et al.* 2013) and sponges (at 400–500 m; Bo *et al.* 2012; Angeletti *et al.* 2020).

Sediments lining the Bari Canyon are formed by sandy muds and muddy sands that are interspersed with large-scale patches of bedrock, coral bioconstructions and patches of biogenic consolidated sediments (Prampolini *et al.* 2021). DAs on the NW slope of the Southern Adriatic shelf are formed by mixtures of autochthonous, relict and reworked Holocene and Pleistocene remains of corals, molluscs and foraminifers (Trincardi *et al.* 2007*a*; Freiwald *et al.* 2009; Tesi *et al.* 2017). Dead *Madrepora, Lophelia* and *Desmophyllum* corals occurring between *c.* 250–585 m range in postmortem age between 230 and 5100 years BP (Taviani *et al.* 2019). The bottom

currents can generate sand waves and lead to reworking and downslope transport of inner-shelf foraminifers (Tesi *et al.* 2017). Molluscan DAs with high levels of bioeroded and encrusted skeletal remains that occur at 200–300 m are represented by Holocene species mixed with the glacial late-Pleistocene species (Panetta *et al.* 2013), including *Pseudamussium septemradiatum,* two specimens of which were dated to 19 000 ± 370 and 15 350 ± 250 cal. years BP (Colantoni 1975; Colantoni and Gallignani 1978; Taviani 1978). Dead shells of *G. vitreus* were also collected in the southern Adriatic Sea between 318 and 616 m (Trincardi *et al.* 2007*a*, 2011), and at two stations sampled during the Poseidon cruise in 2017. The station POS514-14 sampled in the Bari Canyon at 580 m depth is investigated here (Figs 1 & 2). Another station, POS514-26, sampled on the eastern margin of the Southern Adriatic Pit at 509 m also included dead shells of *Gryphus* (black triangles in Fig. 1).

Methods

The station POS514-14 sampled during Poseidon cruise No. 514 in 2017 (41.35002N, 17.19997E, Fig. 2) is located at 580 m water depth on the northern slope of the northern branch of the Bari Canyon (Channel B in Trincardi *et al.* 2007*a*; Angeletti *et al.* 2014), close to a steep, almost vertical wall of the canyon channel. The seafloor at the site is bathed by high-density currents of the North Adriatic Dense Water and is topographically complex with many small depressions. At 580 m, the salinity is equal to 38.8 psu and bottom-water temperature to 13.6–13.8°C (Trincardi *et al.* 2007*b*). Three Van Veen grabs (numbered as 5, 6, and 7) were wet sieved with 1 mm mesh. They all contained dead specimens of *G. vitreus* (Fig. 4). No individuals of *G. vitreus* were collected alive. All *Gryphus* specimens larger than 20 mm ($n = 59$) were immediately picked from grab 6 (labelled as POS514-14-6) during the wet-sieving at the ship, and additional 33 specimens larger than 3 mm were exhaustively picked from the 1/8 of the grab to increase the size coverage of the *G. vitreus* distribution of postmortem ages.

In total, 92 specimens (31 articulated shells, 39 ventral valves, and 22 dorsal valves) were dated with ^{14}C, using the direct carbonate accelerator mass spectrometry (Bush *et al.* 2013). This method is based on powdered carbonate targets and produces

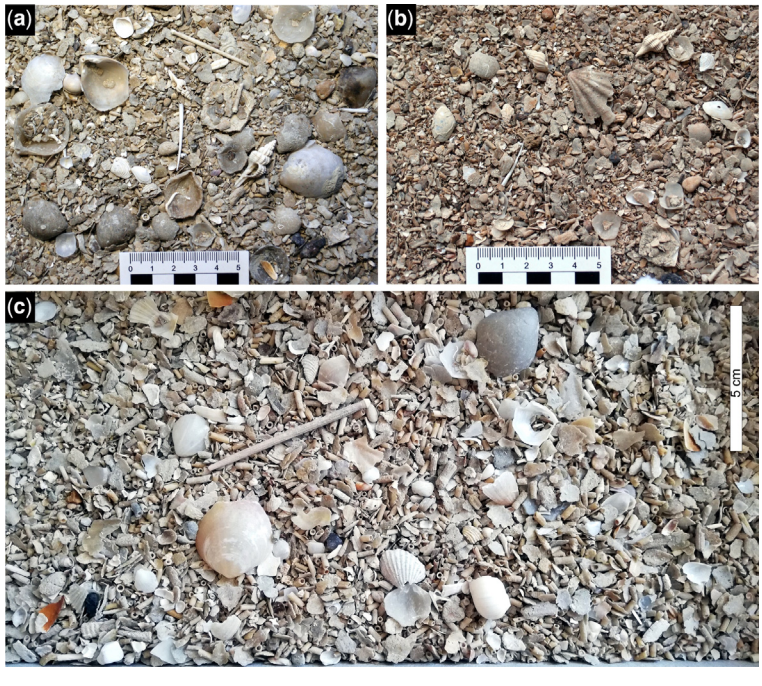

Fig. 4. Skeletal-rich death assemblage residues sieved at 1 mm with tubes of *Ditrupa* and valves of *Gryphus vitreus* collected in three grabs 5, 6 and 7 at 580 m at the station POS514-14 in the Bari Canyon. (**a**) Grab 5; (**b**) grab 7; (**c**) grab 6. The residue of grab 6 lacks articulated shells (>20 mm) that were removed during initial sample sieving and processing at the ship (the photograph captures approx.1/8 of the grab, and thus 4–5 shells of *Gryphus* are missing from it).

postmortem ages that are consistent with the standard graphite ^{14}C method (Bright *et al.* 2021). ^{14}C ages of four specimens range from 7350 to 21 790 ^{14}C years. All the other specimens are younger than 3000 ^{14}C years (with two postbomb ages). Radiocarbon ages were calibrated to calendar ages with the R package rcarbon (Bevan *et al.* 2017). We used the Marine13 database (Reimer *et al.* 2013), with the corresponding ΔR (Reimer and Reimer 2001), and considered the estimate from the southern Adriatic Sea ($\Delta R = 121$ years based on *Mimachlamys varia*, Taviani and Correggiari, in Reimer and McCormac 2002). The calibration results are similar if $\Delta R = 61$ years based on *Glycymeris* shells collected in the central Adriatic Sea (Siani *et al.* 2000). The reservoir age in the Mediterranean Sea was higher by a factor of two during the last deglaciation (Siani *et al.* 2001), but as we focus on shells younger than 3000 years in the quantitative analyses of postmortem age distributions, we used the same ΔR in all calibrations. The calibrated ages are reported in years before present (BP, i.e. before the year 1950, except in analyses of disintegration rates where postmortem ages are rescaled to the time of sampling in AD 2017). Age errors (represented by one standard deviation) of probability distributions of calibrated ages are *c.* 50 years for specimens <1000 years BP, *c.* 80–90 years for specimens that are *c.* 1000–3000 years old, and exceed 100 years for the oldest shells. To assess the effect of these errors on the shape of the distribution, on the location of modes, and on time averaging (measured with an inter-quartile age range, IQR), we estimated postmortem age of each specimen by sampling its age from the calibrated probability age distribution, computed the corresponding frequency of specimens in 50-year cohorts and repeated this sampling 10 000 times. We then estimated the mean frequency (with 95% confidence intervals) of specimens in 50-year cohorts. All radiocarbon and calibrated ages (Supplement A) and the script in R language (R Core Team 2021, Supplement B) are available as supplementary materials.

As postmortem age-frequency distributions of the two subsets of dated shells (59 larger specimens and 33 additional specimens) are similar (bimodal), we pool them in all analyses. In total, 285 specimens of *G. vitreus* (33 shells, 92 dorsal valves, and 160 ventral valves) were exhaustively picked from the grab 6 and 92 of them were dated with ^{14}C. Boullier *et al.* (1986) documented that a shift in the slope of the relationship between shell length and loop length occurs at *c.* 20 mm shell length in *G. vitreus*, and we use this size threshold as an indication that all individuals >20 mm are adults, even when maturity can be achieved at smaller size in similarly-sized brachiopods (Thayer 1977). The resulting size distribution of all shells suggests that most adult individuals >20 mm collected in grab 6 were dated. Therefore, the number of radiocarbon dated individuals exceeding 20 mm effectively corresponds to the total abundance of dead adult specimens in 0.1 m^2 sampled by one Van Veen grab. The preservation of all specimens (disarticulation and completeness of valves) and the presence of encrusters, borers and mineral precipitates on external and internal surfaces were scored under a light microscope at 10–20× magnification. Postmortem age distributions show number of specimens binned to 50-year, and 100-year cohorts (Fig. 5). The relative frequency of articulated shells per cohort (white bars in Fig. 5) is estimated relative to the total number of shells summed with the number of ventral valves in that cohort. The estimation of the location of modes and testing for the bimodality of postmortem age data (with the null hypothesis represented by one mode) follows Ameijeiras-Alonso *et al.* (2019), implemented in Ameijeiras-Alonso *et al.* (2021).

Dead specimens can be lost from the surface sediments of the mixed layer either by disintegration or by burial. This total loss rate controls how the original chronological variability in abundance translates to the distributions of postmortem ages observed in the DA. The internal modes in postmortem age-frequency distribution and the lack or rarity of recently-dead cohorts complicates the estimation of loss rates with taphonomic models that assume temporally-constant production of shells. Here, we account for the decline in abundance by truncating the distribution at the location of the first major pulse at 450 years BP (i.e. prior to the first main peak in the frequency of specimens at *c.* 500 years BP) and at 5000 years BP (i.e. benthic environments were later exposed to the onset and offset of the sapropel phase). We then approximate the loss rate by fitting the postmortem age-frequency distribution (setting postmortem ages relative to the time of sampling, i.e. AD 2017) to a model with a single, temporally-constant rate of loss from the TAZ (i.e. loss rate in the mixed layer does not change with shell postmortem age) and to a model with a temporally-declining rate of loss from the TAZ (i.e. loss rate declines as a dead shells age in the mixed layer), both accounting for abrupt onset and offset in shell production (abruptly-truncated models, Tomašových *et al.* 2016). The first model assumes that disintegration rate in the TAZ and burial rate below the TAZ remain constant in time. The second model postulates that loss rate λ_1 declines to λ_2 at sequestration rate τ. The burial rate of skeletal remains below the surface increment sampled by the Van Veen grab is probably limited at the sampling station because abundant iron-stained skeletal remains and abraded and encrusted intraclasts indicate condensation and very slow net sedimentation rate. Therefore, we neglect the contribution of burial

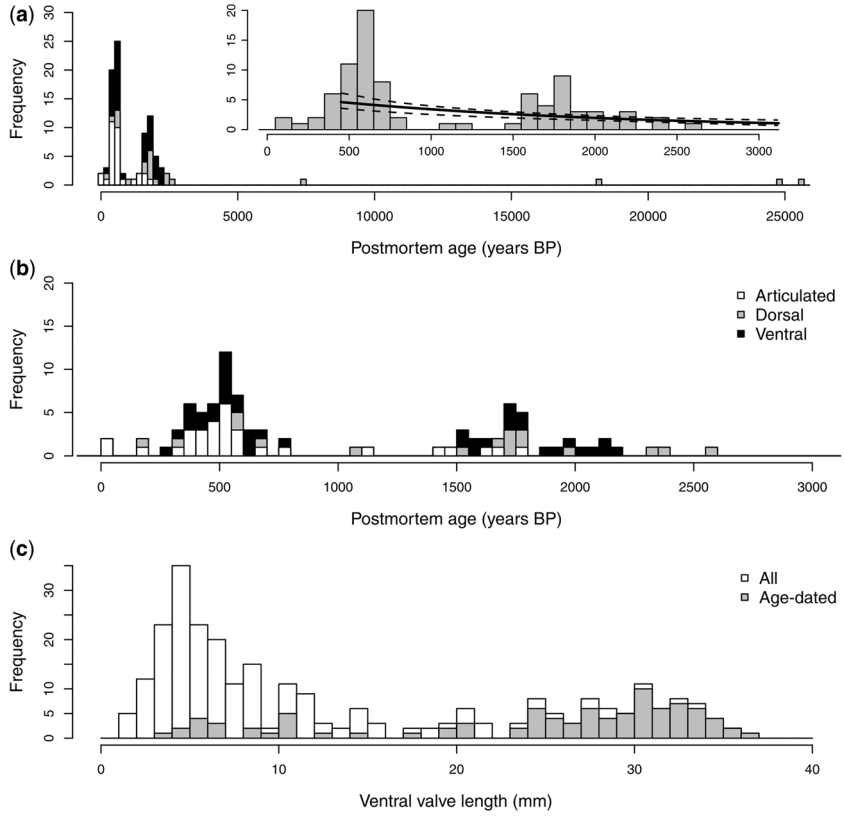

Fig. 5. (**a**) and (**b**) The complete frequency distribution of postmortem ages of *Gryphus vitreus* at POS514-14-6 in 200-year cohorts (a) and the subset (b) showing specimens younger than 3000 years BP in 50-year cohorts, with internal modes at *c.* 500 years and 1750 years BP. Each specimen age corresponds to the median of the probability distribution of calibrated ages. Shading highlights the contribution of articulated shells (white) and disarticulated ventral (black) and dorsal valves (grey). The distributions are based on all dated specimens. The two modes are captured by both articulated and disarticulated specimens, although the contribution of articulated shells diminishes in older cohorts. Both small and large specimens contribute to both modes. The inset in (a) shows the fit of the two taphonomic models to age data that were used to approximate loss rates of specimens from the taphonomic active zone (disintegration rates), truncating the distributions at 450 and 5000 years. (**c**) Size distribution of all *G. vitreus* specimens ($n = 285$) collected in grab 6, with age-dated specimens of *G. vitreus* in grey. The age-dated subset closely captures the mode formed by adult specimens exceeding 20 mm in length.

to loss rate and refer to this loss-rate estimate as disintegration rate (λ) below.

We unmix time-averaged abundance of *G. vitreus* to abundance of specimens produced during 100 years by dividing the counts in 100-year age cohorts by the survival function of the model with temporally-constant rate (the fit of the model with temporally-declining rate to postmortem ages is poor), using the estimate of disintegration half-life derived from the model. The survival function corresponds to $e^{-\lambda t}$ (λ refers to disintegration rate and t refers to time). We scale then these counts to yearly population density within each of the 100-year time bins. The lifespan of *G. vitreus* is unknown, but as the valves at the sampling station possess about ten or more regular growth increments, we assume that the lifespan of adult individuals is *c.* 10 years (similar in magnitude when compared to lifespan of other temperate brachiopods of similar size, Doherty 1979; Baird *et al.* 2013; Baumgarten *et al.* 2014) and discuss the sensitivity of the estimated density if the lifespan would be just 5 years. We use both disintegration models (with temporally-constant and temporally-declining disintegration rate) to (1) visualize the transition between the original time series in abundance and the postmortem age-frequency distribution observed in the surface DAs and to (2) illustrate the procedure of unmixing and scaling of

time-averaged abundance observed in a DA to yearly standing population density expected in a living community.

Models that assume that the original increase and decrease in abundance can be approximated with a symmetric normal-shaped trajectory can be used to evaluate the time-scale of the decline in abundance of *Gryphus*, by estimating the standard deviation of the postmortem age-frequency distribution with the so-called truncated-normal models (Tomašových *et al.* 2016). These models estimate the mean and the standard deviation of the age distribution sourced by a population that exhibited a temporally symmetric trajectory in abundance and was subjected to disintegration in the mixed layer. The mean is a function of (i) the original timing of maximum abundance but also of (ii) disintegration rate and (iii) the rate of change in abundance. However, the standard deviation is just a function of rate of change and is independent of disintegration rate. We fit the so-called truncated-normal model to postmortem ages, using both models of disintegration. We limit this estimation to the last pulse as detected in the death assemblage (i.e. at 500 years BP), and thus exclude specimens older than 1500 years.

Results

DAs in all three grabs are rich in skeletal and intraclastic sand and gravel (Fig. 4). They consist of abundant polychaetes (*Ditrupa*), benthic molluscs (e.g. *Pseudamussium clavatum*, *Abra longicallus*, *Kelliella miliaris, Bathyarca* sp., *Asperarca* sp., anomiid bivalves), pteropods, bryozoans, decapod fragments (*Ebalia nux*), cidaroid spines, benthic foraminifers (e.g. *Ammolagena clavata*), otoliths, and *G. vitreus*. In addition to *Gryphus*, the assemblage also contains disarticulated valves of the micromorphic brachiopod *Platidia anomioides*. Only dead individuals of *G. vitreus* were collected. The time averaging (IQR) of *G. vitreus* specimens is 1250 years, the 90th percentile range is 2170 years (Fig. 5a, b). The median postmortem age is 640 years BP and the mean postmortem age is 1750 years BP. The two youngest specimens represented by articulated shells show postbomb ages. The calibrated ages of the three oldest specimens fall between 18 210–25 620 years BP, and the age of one specimen is 7360 years BP. All other 88 specimens are younger than 3000 years BP (Fig. 5a). The fitting of the model abruptly truncated at 450 and 5000 years BP to postmortem age data (rescaled to AD 2017 so that residence time reflects time since death of individual brachiopods) generates the estimate of disintegration rate λ equal to 0.00055 (i.e. half-life is *c.* 1250 years, Fig. 5a). The fitting of the abruptly-truncated model with temporally-declining disintegration to postmortem age data significantly underestimates the older pulse at 1750 years, and we thus use the model with temporally-constant disintegration in converting time-averaged abundance to annual population density.

For specimens younger than 3000 years BP, the distribution is bimodal (p [H_0 = one mode only] <0.001; p [$H_0 = 2$ modes] $= 0.44$), with the location of the two modes estimated at 510 and 1710 years BP (Fig. 5b). Accounting for the calibration errors, the frequency distribution of specimen postmortem ages binned to 50-year cohorts is also bimodal (Fig. 6), with the mean age of the first mode at 500 years BP (95% c.i. = 460–530 years BP) and of the second mode at 1740 years BP (95% c.i. = 1680–1800 years BP). The 95% confidence intervals on time averaging (IQR) fall between 1190 and 1305 years (Fig. 6). The size-frequency distribution is also bimodal, with abundant juvenile specimens smaller than 10 mm, and with a second mode formed by shells 25–30 mm in length (Fig. 5c).

The truncated-normal model with a temporally-declining disintegration rate (grey lines) fitted to postmortem ages of specimens younger than 1500 years indicates that the standard deviation is 110 years (all specimens) or 120 years (specimens >20 mm). Rate of change in the increase (prior to the younger pulse at *c.* 500 years BP) and in the decline in abundance as fitted by this model thus indicates that most of the decline occurred at the scale of *c.* 100 years, and thus was not protracted over several centuries (grey lines in Fig. 7). This model does not overestimate the abundance of young cohorts, in contrast to the model with a temporally-constant disintegration (black lines in Fig. 7).

Preservation of *G. vitreus* exceeding 15–20 mm is variable, and includes complete shells with loops (brachidia) preserved (Fig. 8a–f), disarticulated but still complete valves with broken loops (Fig. 8g–i), and umbonal fragments that lack peripheral margins and are worn and discoloured, with few worn relicts from the Last Glacial Maximum (Fig. 8j, k). External surfaces of articulated shells are frequently encrusted by foraminifers, serpulids and bryozoans and bored on external surfaces with microendolithic organisms, clionid sponges (*Entobia*), whereas disarticulated valves are encrusted and bioeroded on both sides. A large proportion of old shells (*c.* 500–1800 years BP) is still articulated (white bars in Fig. 5a, b), contain complete loops (Fig. 8a–f) and is frequently internally coated by Mn and Fe oxides, especially along edges of the internal valve surfaces. The relative frequency (percentage) of articulated shells older than 500 years exceeds 50% in several 100-year cohorts (Fig. 5a, b). Small-sized specimens (<20 mm) are rarely articulated. Their preservation ranges from transparent or semi-transparent

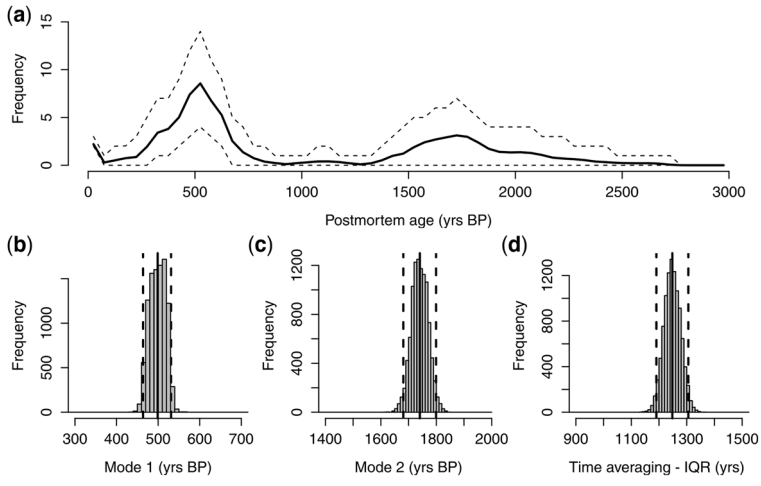

Fig. 6. (**a**) Accounting for the uncertainty in age calibration shows the mean frequency of specimens, with specimen ages binned to 50-year cohorts, predicted by repeated (10 000) sampling of ages from the probability distributions of specimen calibrated ages, with 95% confidence intervals (dashed lines). (**b**)–(**d**) The mean age of the two modes (b–c) and the mean inter-quartile age range (d), with 95% confidence intervals.

complete valves to microbored, encrusted and discoloured valve fragments. The mean postmortem age of articulated shells is 650 years, the mean postmortem age of disarticulated valves with complete outlines is 1236 years, and the mean postmortem age of fragments is 2950 years. The oldest articulated shell is 1771 years old (Fig. 8j, k). The four oldest specimens (>5000 years) are represented by strongly worn and discoloured relicts of the umbonal part of the shell.

Transition from chronological trajectory in abundance to age distribution

Assuming that burial of shells below the TAZ and out-of-habitat transport is negligible, we can model the transition from the original, biphasic chronological series in species abundance to the abundance of postmortem-age cohorts observed in the surface sediment. We specify that two pulses occur at 500 and 1750 years BP, and standard deviation of rate of

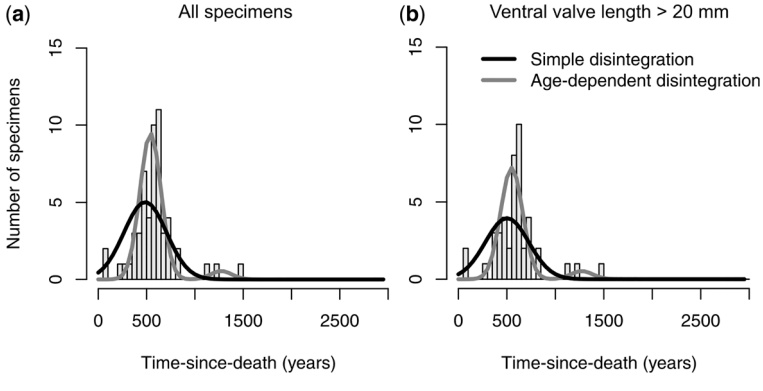

Fig. 7. The truncated-normal model with a temporally-declining disintegration rate (grey lines) fitted to postmortem ages of specimens younger than 1500 years estimates the standard deviation at 110 years (**a**, all specimens) or 120 years (**b**, specimens >20 mm), indicating that the decline in abundance of *Gryphus* occurred at the scale of one century and was thus not protracted over several centuries. (**a**) The truncated-normal models with a temporally-constant disintegration (black lines) overestimate the abundance of the youngest cohort (standard deviation is years on the basis of all specimens and years on the basis of specimens >20 mm).

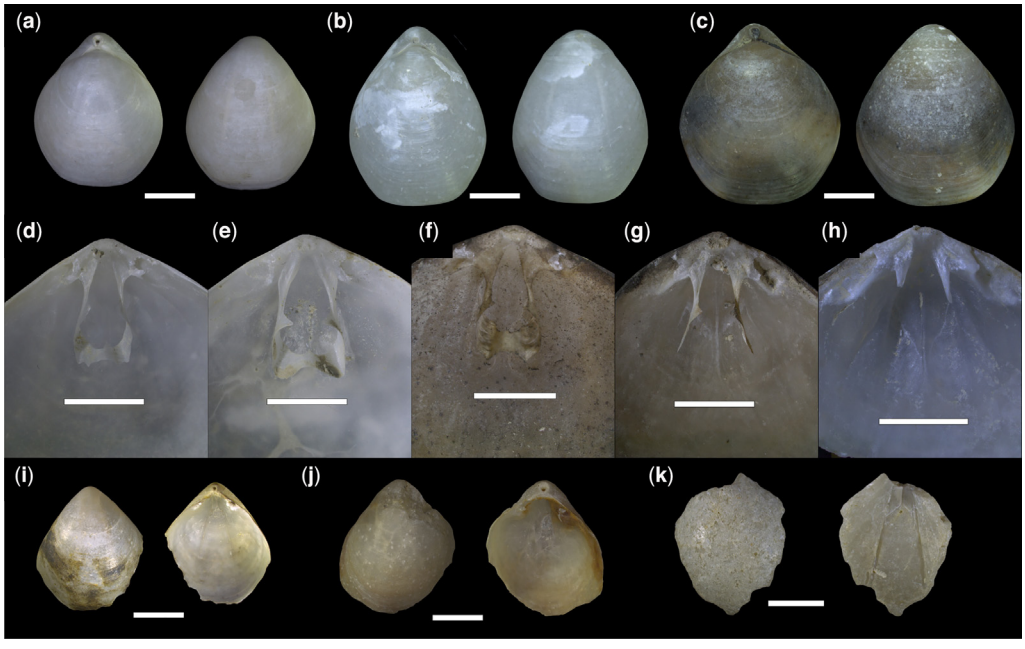

Fig. 8. Preservation states of *Gryphus vitreus*, with (**a–h**) articulated shells with (d–f) complete and (g and h) incomplete loops, (**i** and **j**) disarticulated valves and (**k**) worn umbonal relicts. Specimen numbers and their postmortem ages (BP) follow the letters. (a) 39 (742 years), (b) 4 (406 years), (c) 2 (503 years), (d) 18 (1157 years), (e) 4 (406 years), (f) 2 (503 years), (g) 8 (399 years), (h) 49 (514 years), (i) 49 (514 years), (j) 43-4 (1931 years), (k) 54 (2113 years). Scale bars: (a)–(c), (i), (j) 10 mm; (d)–(h), (k) 5 mm.

change in abundance is equal to 120 (as estimated from empirical data, Fig. 9a, b) and 300 years (to approximate a slower rate of change taking place over several centuries, Fig. 9c, d). These two scenarios are subjected to two preservation regimes (1) with a temporally-constant disintegration rate (Fig. 9a, c) and (2) with a temporal decline in disintegration rate (Fig. 9b, d). As shells located in the TAZ are exposed to disintegration, the original pattern of change in abundance through time is transformed into the DA postmortem age-frequency distribution, in which the number of individuals naturally declines in each age cohort owing to disintegration. The decline is not equal across the cohorts when burial rate is neglected or is smaller than disintegration rate. The abundance of older cohorts is thus penalized by disintegration rate more strongly relative to the abundance of younger cohorts, leading to the smaller abundance of older cohorts in the DA (Fig. 9a–d).

When increasing disintegration half-lives (i.e. the natural logarithm of 2 divided by disintegration rate) from 12 (very fast disintegration) to 1200 years (i.e. as approximated from empirical postmortem age data of all specimens) in the model with temporally-constant disintegration in the mixed layer, an original time series with two abundance pulses occurring at *c.* 500 and 1750 years BP (dashed lines in Fig. 9) is increasingly closer in shape to the distribution expected to be observed in a surface DA (black lines in Fig. 9). The timing of maximum abundance is taphonomically pulled towards the younger cohorts with decreasing disintegration half-life (black arrows on Fig. 9a, c), especially when the temporal decline in abundance is not abrupt (Fig. 9a) but gradual (Fig. 9c). However, when disintegration half-life of shells increases as they reside in the TAZ, the mode shifts towards the younger cohorts only slightly when disintegration half-life exceeds median time to sequestration (Fig. 9b, d, half-time to sequestration is assumed to be 200 years). Only when disintegration half-life is very short (12 years), the resulting distribution is right-skewed, dominated by very young shells, and the original modes disappear (Fig. 9a, c). Long disintegration half-lives in the TAZ thus minimize the bias in the shape of surface postmortem age-frequency distributions relative to the original chronological changes in abundance.

Effects of disintegration rate on temporal variability in abundance of Gryphus

Dividing the counts of shells binned to 100-year cohorts in the observed *Gryphus* distribution of

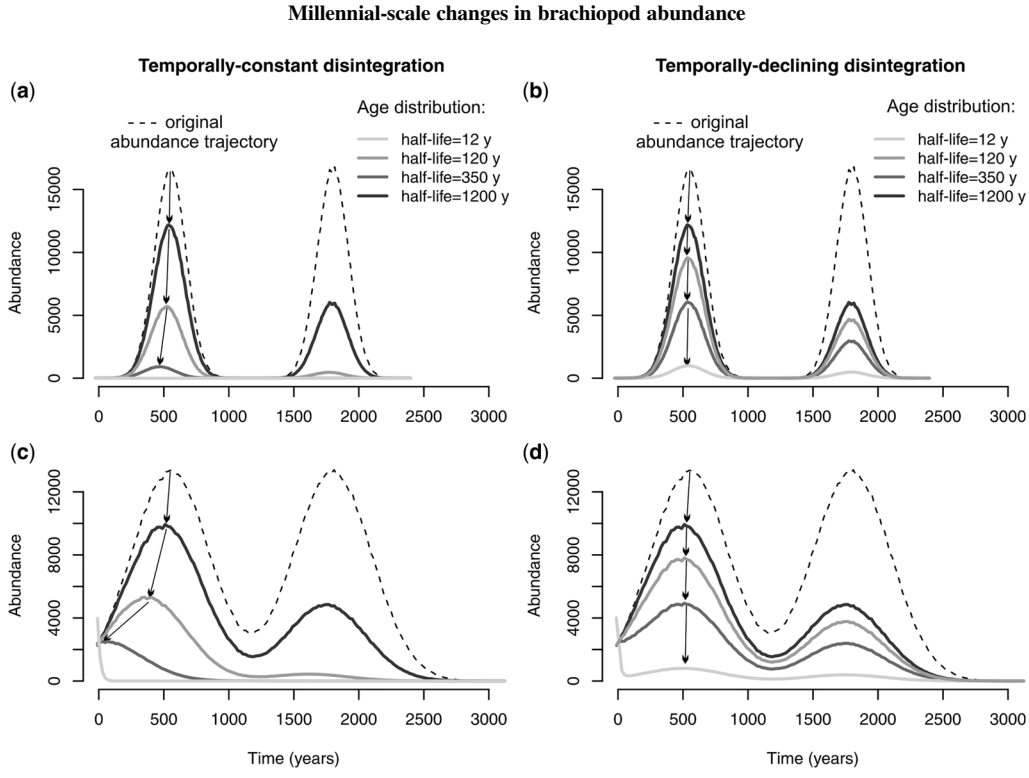

Fig. 9. The effect of shell disintegration rate and rate of change in abundance of living individuals on the shape of age-frequency distributions in the surface death assemblages in two preservation models (a model with the temporally-constant disintegration rate in (a) and (c) and a model with the declining disintegration rate in (b) and (d)). The original chronological trajectory in abundance is defined by two pulses at *c.* 500 years and 1750 years ago (dashed lines), and by a fast (a and b) or slow increase and decline in abundance (c and d). (**a**) and (**b**) Scenario with fast increase and decline in abundance (standard deviation = 120 years, as approximated from empirical age distribution of *Gryphus*). (**c**) and (**d**) Scenario with slower increase and decline in abundance (standard deviation = 300 years). Disintegration half-lives range in four scenarios from 12 to 1200 years in the model with temporally-constant disintegration (a, c). The disintegration half-lives of 12 and 120 years increase to a half-life of 1200 years in all scenarios in the model with age-declining disintegration (b, d). In (a) and especially in (c) where the rate of decline in abundance is slow, the mode of the distribution is visibly pulled towards the youngest cohorts with increasing disintegration rate, i.e. with shorter disintegration half-life (black arrows). In (b) and (d), the mode shifts only slightly unless disintegration half-life becomes very short (12 years), the original modes disappear, and the distribution is right-skewed (half-life = 12 years).

postmortem ages (dashed lines in Fig. 10a, b, based on all dated specimens) by survival function of the two taphonomic models, the reverse procedure occurs, and abundance of individuals in cohorts increases towards the original chronological pattern in abundance. If shells degrade at a temporally-constant rate, with long half-life equal to 1200 years (black lines), the two pulses at 500 and 1750 years BP have similar magnitudes. If half-life declines to 700 years in the model with constant disintegration half-life (grey lines in Fig. 10a), the older pulse is more pronounced than the younger pulse (Fig. 10a). If disintegration half-life increases with increasing postmortem age of shells in the TAZ (Fig. 10b), with the initial decadal-scale half-life of 90 years increasing to 1200 years in all scenarios, the slow sequestration in the model with temporally-declining disintegration rate is equivalent to longer duration of the taphonomic regime with fast disintegration in the model with temporally-constant disintegration half-life. The scenario with slow sequestration thus increases the magnitude of the younger mode relative to that of the older mode, and the original trajectory in abundance thus can be characterized by differences in the magnitude of abundance pulses (black lines, Fig. 10b). When median time to sequestration is similar to disintegration half-life, the difference between the initial trajectory in abundance and the final postmortem age-frequency distribution is smaller (grey lines, Fig. 10b).

In contrast to the model with temporally-constant disintegration rate, very old shells disintegrate at

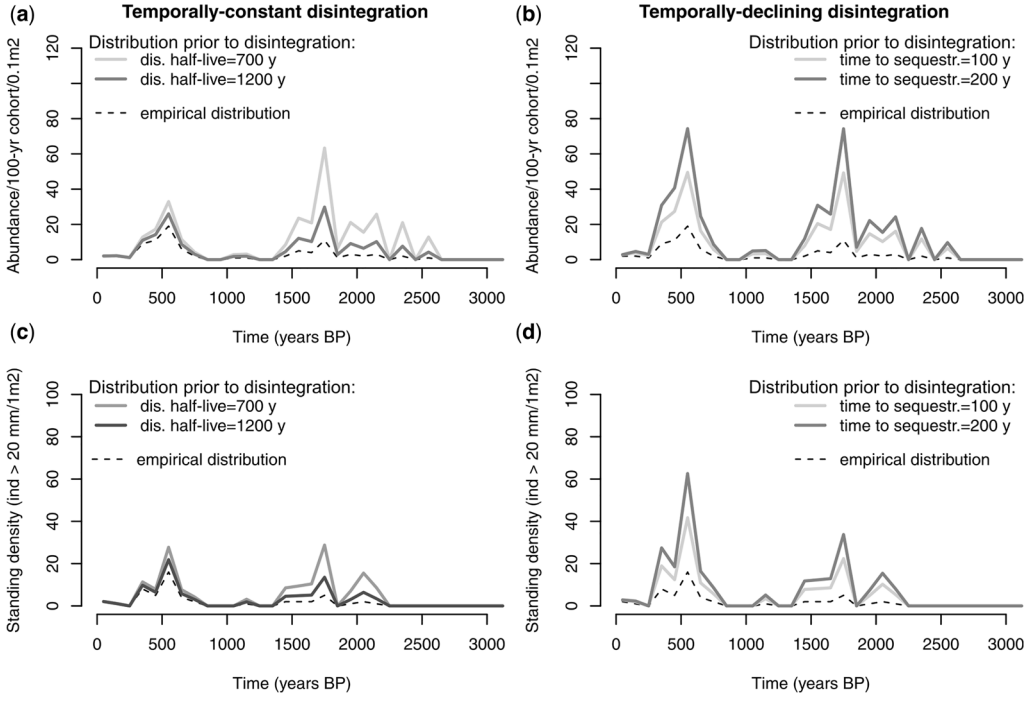

Fig. 10. (**a**) and (**b**) The empirical distribution of *G. vitreus* postmortem ages binned to 100-year cohort (observed in a surface death assemblage) is shown in dashed lines. The modelled distributions (prior to disintegration) in solid and grey lines represent the original trajectories in abundance (computed per 100 years at the scale of grabs, i.e. 0.1 m^2) that generated, under a given combination of disintegration and sequestration rates, the empirical age distributions. In (a) (shells degrade at temporally-constant rate), the pulses at 500 and 1750 years have similar magnitudes in the reconstructed trajectory of abundances when the half-life is 1200 years (black lines). If half-life rate declines to 700 years (grey lines), the older pulse is more pronounced than the younger pulse. In (b) (disintegration declines with shell age, the initial half-life of 90 years increases to 1200 years in all scenarios), the slow sequestration is equivalent to longer duration of the initial phase of disintegration. When time to sequestration is short, the difference between the age distribution and the chronological trajectory in abundance is small. (**c**) and (**d**) Reconstruction of annual population density (per 1 m^2) of *G. vitreus* individuals larger than 20 mm (lifespan = 10 years), in models with temporally-constant disintegration (c) and temporally-declining disintegration (half-life declines from 90 years to 1200 years in all scenarios, (d)). The empirical distribution of postmortem ages is based on the unique number of individuals (shells and ventral valves), with the ventral valve exceeding 20 mm (dashed lines in (c) and (d)).

negligible rate in models with temporally-declining disintegration rate, and the magnitude of older modes (i.e. abundance maxima) thus does not increase in the reconstructions of the original chronological trajectory in abundance of *Gryphus*. These scenarios show that, although the magnitude of modes can shift, depending on the model and the magnitude of disintegration rate, the disintegration alone or its temporal decline does not generate internal modes. Notably, the disintegration rate does not shift the timing of modes in abundance of cohorts markedly (Fig. 10a, b) because the modes of the empirical postmortem age-frequency distribution are relatively sharply separated from the lows. The decline in abundance of *Gryphus* had to take place at the scale of a century (standard deviation of the rate of change in abundance as estimated for the younger pulse is 110–120 years) rather than over several centuries (as in Fig. 9c, d, where abundance was modelled with the standard deviation of 300 years).

Scaling time-averaged abundance to population density

Using the minimum number of individuals (the sum of shells and ventral valves), assuming zero net sedimentation rate, lifespan not shorter than 10 years, and the range of half-lives centred around 1200 years, reconstructing standing densities indicates that populations of adults of *G. vitreus* (exceeding 20 mm) achieved at least *c.* 20 individuals/m^2 at

500 years BP in the Bari Canyon (Fig. 10c). A yearly density of 40–60 individuals/m^2 is predicted when the disintegration half-life of 90 years increases to 1200 years in the course of 100 years (light grey line in Fig. 10d) or 200 years (dark grey line in Fig. 10d). If the half-life of 1200 years also subsumes the loss of specimens below the TAZ by burial, the yearly density is also expected to be higher relative to the initial estimate of 20 individuals/m^2.

Discussion

The effect of disintegration rates on the detection of past abundance fluctuations

The highest abundance of the youngest cohorts and the declining abundance or the lack of older cohorts is a null expectation under steady-state production and any non-negative disintegration or burial rates: it is expected to produce right-skewed, exponential or heavy-tailed frequency distributions of postmortem ages (Olszewski 1999, 2004; Carroll *et al.* 2003). The modelling scenarios in Figures 9 and 10 visualize that high disintegration rates in the TAZ can maximize the bias in the shape of surface postmortem age-frequency distributions relative to the original chronological changes in abundance (with fast sequestration minimizing the bias). The multi-centennial estimate of disintegration half-life generated by fitting the abruptly-truncated taphonomic model to age data (half-life = 1200 years) can be biased upwards because young cohorts are rare, and the initial phase of their residence time in the TAZ potentially characterized by high disintegration cannot be observed. However, as the proportion of articulated shells is very high even in very old cohorts and exceeds 50% in younger age cohorts, we assume that the disintegration half-life of several centuries is not markedly biased up by the rarity of recent *Gryphus* individuals, and that brachiopod disintegration rates at this sampling location are probably very low. All modelling scenarios show that internal modes in abundance of cohorts within surface postmortem age frequency distributions indicate past maxima in abundance of *G. vitreus*.

Subsurface assemblages can be also characterized by internal modes that reflect their time to burial into subsurface layers even when temporal production of shells at the sediment–water interface is constant in time. The exhumation of such subsurface assemblage back to the TAZ (with the original surface sedimentary particles that were overlying the DA with abundant *Gryphus* being fully removed by transport elsewhere, thereby exhuming the *Gryphus* assemblage to the seabed surface) can thus generate a surface assemblage with an internal mode in cohort abundance. However, this scenario with subsurface exhumation of formerly-buried assemblage predicts the lack or rarity of young cohorts of any species. Abundant, well-preserved and delicate bivalve shells of *Kelliella miliaris* and *Abra longicallus* do not show any signs of coatings formed by Fe or Mn oxides in the death assemblage collected at the station POS514-14 (in contrast to well-preserved *Gryphus* shells). Their high abundance in present-day living assemblages in the southern Adriatic Sea (Nasto *et al.* 2018) and their low alteration indicate that these shells are young, and the scenario with full removal of the surface assemblage and the exhumation of older shells from subsurface zones is unlikely. Therefore, we suggest that temporal variability in abundance of *G. vitreus*, driven by changes in the population dynamics is responsible for the presence of two distinct pulses at 500 and 1750 years BP in postmortem age-frequency distributions of *G. vitreus*.

Reconstructing population density

Gryphus presently has not been observed to form any densely-populated beds, patches or aggregations on the seafloor in the Southern Adriatic Sea, in contrast to occurrences in the Western Mediterranean Sea where *Gryphus* forms shell-rich aggregations, with densities between tens and hundreds of living individuals/m^2 (Emig 1989*a*; Grinyó *et al.* 2018). The population density of *Gryphus* in the Mediterranean Sea falls into three categories: (1) 1–5 individuals/m^2 in sparsely-populated habitats (at 110–330 m in the Menorca Channel, Grinyó *et al.* 2018), (2) several tens of individuals/m^2 (in the upper bathyal at 180–250 m off Corsica and Provence), or (3) dense populations exceeding 100s of individuals (at 130–180 m off Corsica and Provence, and at Banc de Magaud near the Hyères Islands, Emig 1987). Multiple camera surveys performed in the Bari Canyon in the twenty-first century did not detect any sites with dense populations of *Gryphus* (D'Onghia *et al.* 2015; Angeletti *et al.* 2019). However, although distributions of postmortem ages indicate that the present-day abundance is smaller than in the past, it is unclear whether the internal modes observed in the distribution of postmortem ages correspond to ecologically-significant population densities equivalent to those observed in the Western Mediterranean Sea today. When time averaging is extensive and disintegration slow, even a species with low standing abundance can become abundant in DAs.

If disintegration were to be neglected, when computing the standing (yearly) density per 1 m^2 on the basis of 100-year cohorts, the division of abundance in each cohort by ten generations (assuming lifespan of 10 years) and the multiplication of the same count by ten (from the scale of Van Veen grab capturing 0.1 m^2 to 1 m^2) would cancel each other out. A

shorter lifespan of 5 years would divide the estimate by half. The resulting estimates of standing densities that do account for disintegration do not markedly differ from those predicted from the raw distribution because the inferred disintegration rates of *Gryphus* are very low (Fig. 10c, d). These estimates of population density are minimum estimates and higher loss by disintegration or other sources of loss by burial or transport to adjacent habitats would imply even higher standing density. To conclude, the estimates of several tens of individuals of *Gryphus* per 1 m^2 indicate that this species was truly abundant at times corresponding to the two modes in the post-mortem age-frequency distribution. These estimates are comparable to intermediate levels of its densities presently observed in the Western Mediterranean Sea.

Ecological causes of volatility

Bathyal benthic communities with epifaunal suspension-feeders in the Southern Adriatic Pit were affected by major multi-millennial variability in deep-water circulation during the Holocene. The bottom currents decreased in velocity at about *c.* 7–10 kyr BP, leading to the deposition of sapropel in the Southern Adriatic Pit (Narciso *et al.* 2012; Tesi *et al.* 2017). Corals re-colonized the Bari Canyon after the sapropel phase (Taviani *et al.* 2019). The distribution of living cold-water corals is asymmetric in the Southern Adriatic Pit during this post-sapropel phase, with higher abundance on the western side (Taviani *et al.* 2019). In the eastern side of this basin, the growth of cold-water corals is sporadic and localized, and most records are based on surface DAs (Angeletti *et al.* 2014, 2015; Nasto *et al.* 2018). However, this turnover related to the onset and offset of the sapropel phase occurred prior to the volatility detected in abundance of *Gryphus* as observed here.

The bathyal communities with *G. vitreus* belong to the EUNIS category (European Nature Information System) 'Communities of bathyal detritic sands with *Gryphus vitreus*' and the LPHME category (Lista Patrón de los Hábitats Marinos Presentes en España) 'Bathyal grounds in the continental shelf edge with *Gryphus vitreus*'. They are considered as vulnerable community types in the Mediterranean Sea negatively affected by deep-water trawl fishing (d'Onghia *et al.* 2003; Maynou and Cartes 2012; Aguilar *et al.* 2017; Carpentieri *et al.* 2021). The Bari Canyon, however, is not subjected to deep-water trawling operations owing to its steep topography (Sion *et al.* 2019), and trawlers primarily operate on the shelf up to 200 m, only occasionally affecting the borders of the canyon (Angeletti *et al.* 2021). The re-suspension of fine-grained sediments produced by trawling on the shelf may trigger increasing siltation of the canyon ecosystems (e.g. Martín *et al.* 2008). However, the bottom trawling activities became industrialized during the second half of the twentieth century in the Adriatic Sea (Fortibuoni *et al.* 2010, 2017; Carpi *et al.* 2017) whereas the decline in abundance of *Gryphus* occurred earlier, as suggested by a relatively fast, centennial-scale decline in abundance after the maximum abundance was achieved at *c.* 500 years BP (Fig. 7).

Siltation and smothering have significant effects on the viability of epifaunal, immobile, suspension-feeding brachiopod populations (Simões *et al.* 2009; Tomašových and Kidwell 2017), even when long-term sedimentation rates are negligible and smothering of living individuals is transient. The Bari Canyon represents a conduit through which suspended fine sediment generated by the Po and other rivers is redistributed southwards along the Italian coast by the predominant count-clockwise circulation pattern (Cattaneo *et al.* 2003), being conveyed into the deeper parts of the Southern Adriatic Pit. The river discharge and sediment load at the prograding deltas sourced by the multitude of rivers that drain the Apennines, and enter into the central Adriatic Sea, increased over the past centuries driven by climatic (with the Last Ice Age phase leading to higher runoff) and anthropogenic changes of the watershed (deforestation and levee construction, Cattaneo *et al.* 2003, 2004, 2007; Correggiari *et al.* 2005*a*, *b*; Stefani and Vincenzi 2005; Mercuri *et al.* 2019). Cattaneo *et al.* (2003, 2007) documented an overall increase in net sedimentation rate over the past 500 years near the Garganto promontory as recorded in sediments of the Garganto subaqueous delta. We hypothesize that these changes led to higher extent of siltation that negatively affected suspension-feeding brachiopods in the Bari Canyon. This hypothesis is supported by the orientation of downward-facing growth forms of corals in the Bari Canyon system that indicates that they avoid the smothering effect (Freiwald *et al.* 2009). Furthermore, sponges in the Bari Canyon are affected by siltation as well (Bo *et al.* 2012), indicating that the currents are not strong enough to remove sediment and to buffer the deleterious effects of siltation. Pedunculate brachiopods such as *Gryphus* with limited repositioning abilities and smaller body size are probably more vulnerable to siltation than epibenthic corals or sponges (Emig 1989*b*).

Changes in deep-water circulation in the Southern Adriatic Sea over the past millennia (Piva *et al.* 2008; Siani *et al.* 2013) may also have led to changes in sediment accumulation and contribute to the volatility of bathyal communities. Piva *et al.* (2008) documented millennial-scale turnovers in the deep-water circulation in the Southern Adriatic Sea owing to changes in the rate of formation and depth of flow of the North Adriatic Dense Water, in response to changes in precipitation intensity

and in the importance of river floods. The two reconstructed peaks in *Gryphus* abundance at *c.* 500 and 1750 years coincide with the former pulses of stronger contribution of the North Adriatic Dense Water to deep-water circulation (at 0.6–0.8 kyr BP and at 1.8–2 kyr BP, Siani *et al.* 2013). Although the dynamics of sediment dispersal and deposition in the Bari Canyon can be decoupled from sediment accumulation induced by river deltas, with sediment sourced from the outer shelf (Tesi *et al.* 2008), the marked expansion in sediment accumulation observed in the mudbelt can be expected to propagate, even with some delay, to bathyal environments. However, as shifts in deep-water circulation coincided with climatic and anthropogenic changes affecting the watersheds and the amount of river-borne sediment discharge along the western Adriatic coast, disentangling the effects of these potential drivers may be difficult. The estimates of postmortem age structure of *Gryphus* assemblages will need to be expanded to other locations and to broader geographical extents to uncover whether the ecological roots of pulses in its abundance in the Bari Canyon is local or regional in scale.

Postmortem age-frequency distributions as the source of information on baseline communities

The conditions with slow disintegration in the TAZ can lead to the formation of relatively complete and unbiased DAs. DAs can efficiently sample patchy or rare species and thus are used in systematic or monitoring surveys to capture long-term abundance structure of regional species pools and spatial distribution patterns (Nebelsick 1996; Bouchet *et al.* 2002; Warwick and Turk 2002; Zuschin and Oliver 2005; Smith 2008; Weber and Zuschin 2013; Powell *et al.* 2017; Casebolt and Kowalewski 2018; Bhattacherjee *et al.* 2021). For example, more than 70% of molluscan species were identified based only on dead shells in monitoring surveys off New Caledonia in habitats deeper than 100 m (Bouchet *et al.* 2009), and the identification of new molluscan species, especially in tropical environments, is frequently based on dead shells (Dijkstra and Maestrati 2010; Dijkstra and Janssen 2013).

The slow shell disintegration rates typical of many marine habitas, however, can represent a challenge for marine biologists and taxonomists that use dead shells as indicators of active inhabitants of the present-day seafloor. In such conditions well-preserved shells can be hundreds to thousands of years old, as articulated shells of *Gryphus* in the death assemblage observed here. Taphonomic clock can be poorly manifested in Holocene brachiopod shells (Carroll *et al.* 2003) when relatively young dead shells are poorly-preserved as they are permanently exposed in the TAZ, whereas some old dead shells can be well-preserved if they have been temporally sequestered below the TAZ and were exhumed to the surface mixed layer only recently. Old *Gryphus* shells tend to be extremely well-preserved and are still articulated, and their good preservation thus does not ensure that they died recently. On the one hand, estimation of post-mortem ages performed in our study shows that well-preserved articulated shells can be misidentified as members of a living local population or a regional species pool in monitoring and taxonomic surveys, thus misrepresenting the current distribution of a species or over-estimating local and regional abundance (Bouchet and Taviani 1992). On the other hand, when taking into account the long-term average of Holocene level-bottom benthic communities inhabiting the Bari Canyon, age dating identifies the temporary dominance of *G. vitreus* at this location during the Late Holocene. Therefore, although the apparently pristine preservation of millennia-old articulated shells of brachiopods can bias systematic or monitoring studies that describe species on the basis of dead shells and attempt to characterize the composition of communities at high temporal resolution, their postmortem age structure expands the utility of surface DAs in tracing the composition of pre-impact baseline communities and identifying their long-term volatility.

Conclusions

Highly time-averaged DAs represent a paradox for conservation palaeobiologists or historical ecologists: although they integrate the total community composition over increasingly longer time-scales, they lose their ability to track ecologically significant volatility. However, the postmortem age structure based on dating of multiple (tens to hundreds) individual shells can effectively detect historical changes over longer, millennial scales, without the need to collect sediment cores, and thus address both the mean composition and its volatility. The DA that consists of largely autochthonous shells uniquely records two pulses of very high abundance of the brachiopod *G. vitreus* in the Bari Canyon during the Late Holocene, in contrast to its present-day rarity. With rapid advances in radiocarbon dating, examination and age dating of dead shells from sample residues collected during surveys of living assemblages, should become a part of the toolkit used in biomonitoring and in identification of baseline communities.

Acknowledgements We thank Marcello G. Simões and an anonymous reviewer for critical reviews. We thank all members of Poseidon cruise No. 514, particularly

chief scientist Hartmut Schulz, Petra Heinz and Tobias B. Grun for help with sampling. We are also grateful to Filip Setena and Angela Scheidl for their help with sample sorting, and Jordon Bright for preparing ^{14}C targets.

Competing interests The authors declare that they have no known competing financial interests or personal relationships that could have appeared to influence the work reported in this paper.

Author contributions **AT**: writing – original draft (equal), writing – review & editing (equal); **DAG-R**: writing – review & editing (equal); **RN**: writing – review & editing (equal); **JHN**: funding acquisition (lead), resources (lead), writing – review & editing (equal); **MZ**: funding acquisition (equal), resources (equal), writing – review & editing (equal).

Funding This research was supported by the Slovak Research and Development Agency (grant no. APVV 17-0555), and the Slovak Scientific Grant Agency (grant no. VEGA 2/0169/19).

Data availability The data and R language scripts are available in the Supplementary Material at https://doi.org/10.6084/m9.figshare.c.6228410.

References

Agiadi, K., Azzarone, M., Hua, Q., Kaufman, D.S., Thivaiou, D. and Albano, P.G. 2022. The taphonomic clock in fish otoliths. *Paleobiology*, **48**, 154–170, https://doi.org/10.1017/pab.2021.30

Aguilar, R., Marín, P. *et al*. 2017. Draft guidelines for inventoring and monitoring of dark habitats. *Thirteenth Meeting of Focal Points for Specially Protected Areas. Agenda Item, vol. 4, United Nations Environment Programme/Mediterranean Action Plan*.

Albano, P.G., Filippova, N., Steger, J., Kaufman, D.S., Tomašových, A., Stachowitsch, M. and Zuschin, M., 2016. Oil platforms in the Persian (Arabian) Gulf: living and death assemblages reveal no effects. *Continental Shelf Research*, **121**, 21–34. https://doi.org/10.1016/j.csr.2015.12.007

Albano, P.G., Hua, Q., Kaufman, D.S., Tomašových, A., Zuschin, M. and Agiadi, K. 2020. Radiocarbon dating supports bivalve-fish age coupling along a bathymetric gradient in high-resolution paleoenvironmental studies. *Geology*, **48**, 589–593, https://doi.org/10.1130/G47210.1

Ameijeiras-Alonso, J., Crujeiras, R.M. and Rodríguez-Casal, A. 2019. Mode testing, critical bandwidth and excess mass. *Test*, **28**, 900–919, https://doi.org/10.1007/s11749-018-0611-5

Ameijeiras-Alonso, J., Crujeiras, R.M. and Rodríguez-Casal, A. 2021. Multimode: an R Package for Mode Assessment. *Journal of Statistical Software*, **97**, 1–32, https://doi.org/10.18637/jss.v097.i09

Angeletti, L. and Taviani, M. 2011. Entrapment, preservation and incipient fossilization of benthic predatory molluscs within deep-water coral frames in the Mediterranean Sea. *Geobios*, **44**, 543–548, https://doi.org/10.1016/j.geobios.2011.02.004

Angeletti, L., Taviani, M. *et al*. 2014. New deep-water cnidarian sites in the southern Adriatic Sea. *Mediterranean Marine Science*, **15**, 263–273, https://doi.org/10.12681/mms.558

Angeletti, L., Canese, S., Franchi, F., Montagna, P., Reitner, J., Walliser, E.O. and Taviani, M. 2015. The 'chimney forest' of the deep Montenegrin margin, south-eastern Adriatic Sea. *Marine Petroleum Geology*, **66**, 542–554, https://doi.org/10.1016/j.marpetgeo.2015.04.001

Angeletti, L., Bargain, A. *et al*. 2019. Cold-water coral multiscale habitat mapping: methodologies and perspectives. *In*: Orejas, C. and Jiménez, C. (eds) *Mediterranean Cold-Water Corals: Past, Present and Future*. Springer International, Berlin, 173–189.

Angeletti, L., Prampolini, M., Foglini, F., Grande, V. and Taviani, M. 2020. Cold-water coral habitat in the Bari Canyon System, Southern Adriatic Sea (Mediterranean Sea). *In*: Harris, P. and Baker, E. (eds) *Seafloor Geomorphology as Benthic Habitat*. Elsevier, 811–824.

Angeletti, L., D'Onghia, G., Otero, M.D.M., Settanni, A., Spedicato, M.T. and Taviani, M. 2021. A perspective for best governance of the Bari Canyon deep-sea ecosystems. *Water*, **16**, 1646, https://doi.org/10.3390/w13121646

Baco, A.R., Morgan, N., Roark, E.B., Silva, M., Shamberger, K.E. and Miller, K. 2017. Defying dissolution: discovery of deep-sea scleractinian coral reefs in the North Pacific. *Scientific Reports*, **7**, 1–11, https://doi.org/10.1038/s41598-016-0028-x

Baird, M.J., Lee, D.E. and Lamare, M.D. 2013. Reproduction and growth of the terebratulid brachiopod *Liothyrella neozelanica* Thomson, 1918 from Doubtful Sound, New Zealand. *Biological Bulletin*, **225**, 125–136, https://doi.org/10.1086/BBLv225n3p125

Baumgarten, S., Laudien, J., Jantzen, C., Häussermann, V. and Försterra, G. 2014. Population structure, growth and production of a recent brachiopod from the Chilean fjord region. *Marine Ecology*, **35**, 401–413, https://doi.org/10.1111/maec.12097

Bevan, A., Crema, E., Boncinsky, R.K., Hinz, M., Riris, P. and Silva, F. 2017. Rcarbon: Calibration and analysis of radiocarbon dates. R package version, 1, github.com/ahb108/rcarbon/

Bhattacherjee, M., Chattopadhyay, D., Som, B., Sankar, A.S. and Mazumder, S. 2021. Molluscan live-dead fidelity of a storm-dominated shallow-marine setting and its implications. *Palaios*, **36**, 77–93, https://doi.org/10.2110/palo.2020.020

Bo, M., Bertolino, M. *et al*. 2012. Role of deep sponge grounds in the Mediterranean Sea: a case study in southern Italy. *Hydrobiologia*, **687**, 163–177, https://doi.org/10.1007/s10750-011-0964-1

Bouchet, P. and Taviani, M. 1992. The Mediterranean deep-sea fauna: pseudopopulations of Atlantic species? *Deep Sea Research Part A Oceanographic Research Papers*, **39**, 169–184, https://doi.org/10.1016/0198-0149(92)90103-Z

Bouchet, P., Lozouet, P., Maestrati, P. and Heros, V. 2002. Assessing the magnitude of species richness in tropical marine environments: exceptionally high numbers of molluscs at a New Caledonia site. *Biological Journal*

of the Linnean Society, **75**, 421–436, https://doi.org/10.1046/j.1095-8312.2002.00052.x

Bouchet, P., Lozouet, P. and Sysoev, A. 2009. An inordinate fondness for turrids. *Deep Sea Research Part II: Topical Studies in Oceanography*, **56**, 1724–1731, https://doi.org/10.1016/j.dsr2.2009.05.033

Boullier, A., Delance, J.H., Emig, C.C., d'Hondt, J.L., Gaspard, D. and Laurin, B. 1986. Les populations de *Gryphus vitreus* (Brachiopoda) en Corse. Implications paléontologiques. *Biostratigraphie du Paléozoïque*, **4**, 179–196.

Bright, J., Ebert, C. *et al*. 2021. Comparing direct carbonate and standard graphite ^{14}C determinations of biogenic carbonates. *Radiocarbon*, **63**, 387–403, https://doi.org/10.1017/RDC.2020.131

Brunton, C.H.C. 1988. Some brachiopods from the eastern Mediterranean Sea. *Israel Journal of Ecology and Evolution*, **35**, 151–169.

Bush, S.L., Santos, G.M., Xu, X., Southon, J.R., Thiagarajan, N., Hines, S.K. and Adkins, J.F. 2013. Simple, rapid, and cost effective: a screening method for ^{14}C analysis of small carbonate samples. *Radiocarbon*, **55**, 631–640, https://doi.org/10.1017/S0033822200057787

Carpentieri, P., Nastasi, A., Sessa, M. and Srour, A. 2021. Incidental catch of vulnerable species in Mediterranean and Black Sea fisheries a review. *General Fisheries Commission for the Mediterranean Studies and Reviews*, **101**, 1–317, https://doi.org/10.4060/cb5405en

Carpi, P., Scarcella, G. and Cardinale, M. 2017. The saga of the management of fisheries in the Adriatic Sea: history, flaws, difficulties, and successes toward the application of the common fisheries policy in the Mediterranean. *Frontiers Marine Science*, **4**, 423, https://doi.org/10.3389/fmars.2017.00423

Carroll, M., Kowalewski, M., Simões, M.G. and Goodfriend, G.A. 2003. Quantitative estimates of time-averaging in terebratulid brachiopod shell accumulations from a modern tropical shelf. *Paleobiology*, **29**, 381–402, https://doi.org/10.1666/0094-8373(2003)029<0381:QEOTIT>2.0.CO;2

Cartes, J.E., Maynou, F., Fanelli, E., Romano, C., Mamouridis, V. and Papiol, V. 2009. The distribution of megabenthic, invertebrate epifauna in the Balearic Basin (western Mediterranean) between 400 and 2300 m: environmental gradients influencing assemblages composition and biomass trends. *Journal of Sea Research*, **61**, 244–257, https://doi.org/10.1016/j.seares.2009.01.005

Casebolt, S. and Kowalewski, M. 2018. Mollusk shell assemblages as archives of spatial structuring of benthic communities around subtropical islands. *Estuarine, Coastal and Shelf Science*, **215**, 132–143, https://doi.org/10.1016/j.ecss.2018.09.023

Cattaneo, A., Correggiari, A., Langone, L. and Trincardi, F. 2003. The late-Holocene Gargano subaqueous delta, Adriatic shelf: sediment pathways and supply fluctuations. *Marine Geology*, **193**, 61–91, https://doi.org/10.1016/S0025-3227(02)00614-X

Cattaneo, A., Trincardi, F., Langone, L., Asioli, A. and Puig, P. 2004. Clinoform generation on Mediterranean margins. *Oceanography*, **17**, 105–117, https://doi.org/10.5670/oceanog.2004.08

Cattaneo, A., Trincardi, F., Asioli, A. and Correggiari, A. 2007. The Western Adriatic shelf clinoform: energy-limited bottomset. *Continental Shelf Research*, **27**, 506–525, https://doi.org/10.1016/j.csr.2006.11.013

Chaikin, S., Dubiner, S. and Belmaker, J. 2022. Cold-water species deepen to escape warm water temperatures. *Global Ecology and Biogeography*, **31**, 75–88, https://doi.org/10.1111/geb.13414

Colantoni, P. 1975. Prime datazioni assolute di una fauna fossile a *Pseudamussium septemradiatum* dragata nel basso Adriatico. *Giornale di Geologia*, **40**, 133–140

Colantoni, P. and Gallignani, P. 1978. Quaternary evolution of the continental shelf off the coast of Bari (South Adriatic Sea): shallow seismic, sedimentological and faunal evidences. *Géologie Méditerranéenne*, **5**, 327–338, https://doi.org/10.3406/geolm.1978.1054

Correggiari, A., Cattaneo, A. and Trincardi, F. 2005*a*. The modern Po Delta system: lobe switching and asymmetric prodelta growth. *Marine Geology*, **222**, 49–74, https://doi.org/10.1016/j.margeo.2005.06.039

Correggiari, A., Cattaneo, A. and Trincardi, F. 2005*b*. Depositional patterns in the late Holocene Po delta system. *SEPM Society for Sedimentary Geology*, **83**, 365–392.

Cox, I. 1934. Notes on the shell musculature of *Gryphus vitreus* (Born). *Geological Magazine*, **71**, 226–230, https://doi.org/10.1017/S0016756800093171

Davies, D.J., Powell, E.N. and Stanton, R.J., Jr. 1989. Relative rates of shell dissolution and net sediment accumulation-a commentary: can shell beds form by the gradual accumulation of biogenic debris on the sea floor? *Lethaia*, **22**, 207–212, https://doi.org/10.1111/j.1502-3931.1989.tb01683.x

Delance, J.H. and Emig, C.C. 2004. Drilling predation on *Gryphus vitreus* (Brachiopoda) off the French Mediterranean coasts. *Palaeogeography, Palaeoclimatology, Palaeoecology*, **208**, 23–30, https://doi.org/10.1016/j.palaeo.2004.02.025

Dexter, T.A., Kaufman, D.S. *et al*. 2014. A continuous multi-millennial record of surficial bivalve mollusk shells from the São Paulo Bight, Brazilian shelf. *Quaternary Research*, **81**, 274–283, https://doi.org/10.1016/j.yqres.2013.12.007

Doherty, P.J. 1979. A demographic study of a subtidal population of the New Zealand articulate brachiopod *Terebratella inconspicua*. *Marine Biology*, **52**, 331–342, https://doi.org/10.1007/BF00389074

Dijkstra, H.H. and Janssen, R. 2013. Bathyal and abyssal Pectinoidea from the Red Sea and Gulf of Aden (Bivalvia: Propeamussiidae, Entoliidae, Pectinidae). *Archiv für Molluskenkunde: International Journal of Malacology*, **142**, 181–214, https://doi.org/10.1127/arch.moll/1869-0963/142/181-214

Dijkstra, H.H. and Maestrati, P. 2010. Pectinoidea (Mollusca, Bivalvia, Propeamussiidae, Entoliidae and Pectinidae) from the Austral Islands (French Polynesia). *Zoosystema*, **32**, 333–358, https://doi.org/10.5252/z2010n2a6

Delibrias, G. and Taviani, M. 1984. Dating the death of Mediterranean deep-sea scleractinian corals. *Marine Geology*, **62**, 175–180, https://doi.org/10.1016/0025-3227(84)90062-8

Dominici, S. and Zuschin, M. 2005. Infidelities of fossil assemblages. *Lethaia*, **38**, 381–382, https://doi.org/10.1080/00241160500289518

D'Onghia, G., Mastrototaro, F., Matarrese, A., Politou, C. and Mytilineou, C. 2003. Biodiversity of the upper slope demersal community in the eastern Mediterranean: preliminary comparison between two areas with and without trawl fishing. *Journal of Northwest Atlantic Fishery Science*, **31**, 263–273, https://doi.org/10.2960/J.v31.a20

D'Onghia, G., Capezzuto, F. *et al*. 2015. Macro- and megafauna recorded in the submarine Bari Canyon (southern Adriatic, Mediterranean Sea) using different tools. *Mediterranean Marine Science*, **16**, 180–196, https://doi.org/10.12681/mms.1082

Edinger, E.N. and Sherwood, O.A. 2012. Applied taphonomy of gorgonian and antipatharian corals in Atlantic Canada: experimental decay rates, field observations, and implications for assessing fisheries damage to deep-sea coral habitats. *Neues Jahrbuch fur Geologie und Palaontologie-Abhandlungen*, **265**, 199–218, https://doi.org/10.1127/0077-7749/2012/0255

Emig, C.C. 1985. Distribution et synécologie des fonds à *Gryphus vitreus* (Brachiopoda) en Corse. *Marine Biology*, **90**, 139–146, https://doi.org/10.1007/BF00428225

Emig, C.C. 1987. Offshore brachiopods investigated by submersible. *Journal of Experimental Marine Biology and Ecology*, **108**, 261–273, https://doi.org/10.1016/0022-0981(87)90089-X

Emig, C.C. 1989*a*. Distributional patterns along the Mediterranean continental margin (Upper Bathyal) using *Gryphus vitreus* (Brachiopoda) densities. *Palaeogeography, Palaeoclimatology, Palaeoecology*, **71**, 253–256, https://doi.org/10.1016/0031-0182(89)90053-9

Emig, C.C. 1989*b*. Observations préliminaires sur l'envasement de la biocoenose à *Gryphus vitreus* (Brachiopoda), sur la pente continentale du Nord de la Corse (Méditerranée). Origines et conséquences. *Comptes Rendus de l'Académie des Sciences Paris*, **309**, 337–342.

Emig, C.C. 1990. Examples of post-mortality alteration in Recent brachiopod shells and (paleo) ecological consequences. *Marine Biology*, **104**, 233–238. https://doi.org/10.1007/BF01313263

Fabri, M.C., Pedel, L., Beuck, L., Galgani, F., Hebbeln, D. and Freiwald, A. 2014. Megafauna of vulnerable marine ecosystems in French mediterranean submarine canyons: spatial distribution and anthropogenic impacts. *Deep Sea Research Part II: Topical Studies in Oceanography*, **104**, 184–207, https://doi.org/10.1016/j.dsr2.2013.06.016

Fernandez-Arcaya, U., Ramirez-Llodra, E. *et al*. 2017. Ecological role of submarine canyons and need for canyon conservation: a review. *Frontiers in Marine Science*, **4**, https://doi.org/10.3389/fmars.2017.00005

Flessa, K.W., Cutler, A.H. and Meldahl, K.H. 1993. Time and taphonomy: quantitative estimates of time-averaging and stratigraphic disorder in a shallow marine habitat. *Paleobiology*, **19**, 266–286, https://doi.org/10.1017/S0094837300015918

Foglini, F., Campiani, E. and Trincardi, F. 2016. The reshaping of the South West Adriatic Margin by cascading of dense shelf waters. *Marine Geology*, **375**, 64–81, https://doi.org/10.1016/j.margeo.2015.08.011

Fortibuoni, T., Libralato, S., Raicevich, S., Giovanardi, O. and Solidoro, C. 2010. Coding early naturalists' accounts into long-term fish community changes in the Adriatic Sea (1800–2000). *PloS One*, **5**, e15502, https://doi.org/10.1371/journal.pone.0015502

Fortibuoni, T., Libralato, S., Arneri, E., Giovanardi, O., Solidoro, C. and Raicevich, S. 2017. Fish and fishery historical data since the nineteenth century in the Adriatic Sea, Mediterranean. *Scientific Data*, **4**, 170104, https://doi.org/10.1038/sdata.2017.104

Freiwald, A., Beuck, L., Rüggeberg, A., Taviani, M. and Hebbeln, D. 2009. The white coral community in the central Mediterranean Sea revealed by ROV surveys. *Oceanography*, **22**, 58–74, https://doi.org/10.5670/oceanog.2009.06

Gamulin-Brida, H. 1983. Crnogorsko primorje-specifični dio Jadrana s gledišta bentoskih biocenoza i njihove zaštite. *Studia Marina*, **13–14**, 205–214.

Gaspard, D. 1989. Quelques aspects de la biodegradation des coquilles de brachiopodes; consequences sur leur fossilisation. *Bulletin de la Société géologique de France*, **6**, 1207–1216, https://doi.org/10.2113/gssgfbull.V.6.1207

Gaspard, D. 2011. Endolithic algae, fungi and bacterial activity in Holocene and Cretaceous brachiopod shells-diagenetic consequences. *Memoirs of the Association of Australasian Palaeontologists*, **41**, 327–337, search.informit.org/doi/epdf/10.3316/informit.655577756172395

Gaspard, D., Marin, F., Guichard, N., Morel, S., Alcaraz, G. and Luquet, G. 2007. Shell matrices of Recent rhynchonelliform brachiopods: microstructures and glycosylation studies. *Earth and Environmental Science Transactions of the Royal Society of Edinburgh*, **98**, 415–424, https://doi.org/10.1017/S1755691007078401

Georgian, S.E., Dupont, S., Kurman, M., Butler, A., Strömberg, S.M., Larsson, A.I. and Cordes, E.E. 2016. Biogeographic variability in the physiological response of the cold-water coral *Lophelia pertusa* to ocean acidification. *Marine Ecology*, **37**, 1345–1359, https://doi.org/10.1111/maec.12373

Gönülal, O. and Güresen, O. 2014. A list of macrofauna on the continental shelf of Gökçeada Island (northern Aegean Sea) with a new record (*Gryphus vitreus* Born, 1778) (Brachiopoda, Rhynchonellata) for the Türkish seas. *Journal of Black Sea/Mediterranean Environment*, **20**, 228–252, https://blackmeditjournal.org/wp-content/uploads/2014_vol_20_no3-5.pdf

Grinyó, J., Gori, A. *et al*. 2018. Megabenthic assemblages in the continental shelf edge and upper slope of the Menorca Channel, Western Mediterranean Sea. *Progress in Oceanography*, **162**, 40–51, https://doi.org/10.1016/j.pocean.2018.02.002

Jonkers, L., Hillebrand, H. and Kucera, M. 2019. Global change drives modern plankton communities away from the pre-industrial state. *Nature*, **570**, 372–375, https://doi.org/10.1038/s41586-019-1230-3

Kidwell, S.M. 2007. Discordance between living and death assemblages as evidence for anthropogenic ecological change. *Proceedings of the National Academy of Sciences*, **104**, 17701–17706, https://doi.org/10.1073/pnas.0707194104

Kidwell, S.M. 2008. Ecological fidelity of open marine molluscan death assemblages: effects of post-mortem transportation, shelf health, and taphonomic inertia.

Lethaia, **41**, 199–217, https://doi.org/10.1111/j.1502-3931.2007.00050.x

Kidwell, S.M., Best, M.M. and Kaufman, D.S. 2005. Taphonomic trade-offs in tropical marine death assemblages: differential time averaging, shell loss, and probable bias in siliciclastic v. carbonate facies. *Geology*, **33**, 729–732, https://doi.org/10.1130/G21607.1

Kosnik, M.A., Hua, Q., Jacobsen, G.E., Kaufman, D.S. and Wüst, R.A. 2007. Sediment mixing and stratigraphic disorder revealed by the age-structure of *Tellina* shells in Great Barrier Reef sediment. *Geology*, **35**, 811–814, https://doi.org/10.1130/G23722A.1

Kosnik, M.A., Hua, Q., Kaufman, D.S. and Wüst, R.A. 2009. Taphonomic bias and time-averaging in tropical molluscan death assemblages: differential shell half-lives in Great Barrier Reef sediment. *Paleobiology*, **35**, 565–586, https://doi.org/10.1666/0094-8373-35.4.565

Kosnik, M.A., Kaufman, D.S. and Hua, Q. 2013. Radiocarbon-calibrated multiple amino acid geochronology of Holocene molluscs from Bramble and Rib Reefs (Great Barrier Reef, Australia). *Quaternary Geochronology*, **16**, 73–86, https://doi.org/10.1016/j.quageo.2012.04.024

Krause, R.A., Barbour, S.L., Kowalewski, M., Kaufman, D.S., Romanek, C.S., Simoes, M.G. and Wehmiller, J.F. 2010. Quantitative comparisons and models of time-averaging in bivalve and brachiopod shell accumulations. *Paleobiology*, **36**, 428–452, https://doi.org/10.1666/08072.1

Kowalewski, M., Serrano, G.E.A., Flessa, K.W. and Goodfriend, G.A. 2000. Dead delta's former productivity: two trillion shells at the mouth of the Colorado River. *Geology*, **28**, 1059–1062, https://doi.org/10.1130/0091-7613(2000)28<1059:DDFPTT>2.0.CO;2

Logan, A., Bianchi, C.N., Morri, C.A.R.L.A., Zibrowius, H. and Bitar, G. 2002. New records of Recent brachiopods from the eastern Mediterranean Sea. *Annali del Museo civico di Storia naturale" G Doria*, **94**, 407–418.

Maier, C., Watremez, P., Taviani, M., Weinbauer, M.G. and Gattuso, J.P. 2012. Calcification rates and the effect of ocean acidification on Mediterranean cold-water corals. *Proceedings of the Royal Society B: Biological Sciences*, **279**, 1716–1723, https://doi.org/10.1098/rspb.2011.1763

Maier, C., Schubert, A., Berzunza Sànchez, M.M., Weinbauer, M.G., Watremez, P. and Gattuso, J.P. 2013. End of the century pCO2 levels do not impact calcification in Mediterranean cold-water corals. *PloS One*, **8**, e62655, https://doi.org/10.1371/journal.pone.0062655

Marano, G., Ungaro, N. and Vaccarella, R. 1989. Nota preliminare sulle comunità di macroinvertebrati dei fondi strascicabili dell'Adriatico pugliese. *Thalassia Salentina*, **19**, 3–19.

Margolin, A.R., Robinson, L.F. *et al*. 2014. Temporal and spatial distributions of cold-water corals in the Drake Passage: insights from the last 35 000 years. *Deep Sea Research Part II: Topical Studies in Oceanography*, **99**, 237–248, https://doi.org/10.1016/j.dsr2.2013.06.008

Martín, J., Puig, P., Palanques, A., Masqué, P. and García-Orellana, J. 2008. Effect of commercial trawling on the deep sedimentation in a Mediterranean submarine canyon. *Marine Geology*, **252**, 150–155, https://doi.org/10.1016/j.margeo.2008.03.012

Mastrototaro, F., d'Onghia, G. *et al*. 2010. Biodiversity of the white coral bank off Cape Santa Maria di Leuca (Mediterranean Sea): an update. *Deep Sea Research Part II: Topical Studies in Oceanography*, **57**, 412–430, https://doi.org/10.1016/j.dsr2.2009.08.021

Maynou, F. and Cartes, J.E. 2012. Effects of trawling on fish and invertebrates from deep-sea coral facies of Isidella elongata in the western Mediterranean. *Journal of the Marine Biological Association of the United Kingdom*, **92**, 1501–1507, https://doi.org/10.1017/S0025315411001603

Mercuri, A.M., Florenzano, A., Terenziani, R., Furia, E., Dallai, D. and Torri, P. 2019. Middle-to late-Holocene fire history and the impact on Mediterranean pine and oak forests according to the core RF93-30, central Adriatic Sea. *Holocene*, **29**, 1362–1376, https://doi.org/10.1177/0959683619846982

Middelburg, J.J., Soetaert, K. and Herman, P.M. 1997. Empirical relationships for use in global diagenetic models. *Deep Sea Research Part I: Oceanographic Research Papers*, **44**, 327–344, https://doi.org/10.1016/S0967-0637(96)00101-X

Moffitt, S.E., Hill, T.M., Roopnarine, P.D. and Kennett, J.P. 2015. Response of seafloor ecosystems to abrupt global climate change. *Proceedings of the National Academy of Sciences*, **112**, 4684–4689, https://doi.org/10.1073/pnas.1417130112

Morato, T., González-Irusta, J.M. *et al*. 2020. Climate-induced changes in the suitable habitat of cold-water corals and commercially important deep-sea fishes in the North Atlantic. *Global Change Biology*, **26**, 2181–2202, https://doi.org/10.1111/gcb.14996

Narciso, Á., Flores, J.A., Cachão, M., Piva, A., Asioli, A., Andersen, N. and Schneider, R. 2012. Late Glacial–Holocene transition in the southern Adriatic Sea: Coccolithophore and Foraminiferal evidence. *Micropaleontology*, **58**, 523–538, https://doi.org/10.47894/mpal.58.6.04

Nasto, I., Cardone, F. *et al*. 2018. Benthic invertebrates associated with subfossil cold-water coral frames and hardgrounds in the Albanian deep waters (Adriatic Sea). *Turkish Journal of Zoology*, **42**, 360–371, https://doi.org/10.3906/zoo-1708-44

Nebelsick, J.H. 1996. Biodiversity of shallow-water Red Sea echinoids: implications for the fossil record. *Journal of the Marine Biological Association of the United Kingdom*, **76**, 185–194, https://doi.org/10.1017/S0025315400029118

Noé, S., Titschack, J., Freiwald, A. and Dullo, W.C. 2006. From sediment to rock: diagenetic processes of hardground formation in deep-water carbonate mounds of the NE Atlantic. *Facies*, **52**, 183–208, https://doi.org/10.1007/s10347-005-0037-x

Olszewski, T. 1999. Taking advantage of time-averaging. *Paleobiology*, **25**, 226–238, https://doi.org/10.1017/S009483730002652X

Olszewski, T.D. 2004. Modeling the influence of taphonomic destruction, reworking, and burial on time-averaging in fossil accumulations. *Palaios*, **19**, 39–50, https://doi.org/10.1669/0883-1351(2004)019<0039:MTIOTD>2.0.CO;2

Olszewski, T.D. and Kaufman, D.S. 2015. Tracing burial history and sediment recycling in a shallow estuarine setting (Copano Bay, Texas) using postmortem ages

of the bivalve *Mulinia lateralis*. *Palaios*, **30**, 224–237, https://doi.org/10.2110/palo.2014.063

Panetta, P., Mastrototaro, F., Chimienti, G., Angeletti, L., D'Onghia, G. 2013. Tanatocenosi Wurmiana nel Canyon di Bari (Mar Adriatico). *Biologia Marina Mediterranea*, **20**, 148–149.

Perry, C.T. and Smithers, S.G. 2011. Cycles of coral reef 'turn-on', rapid growth and 'turn-off' over the past 8500 years: a context for understanding modern ecological states and trajectories. *Global Change Biology*, **17**, 76–86, https://doi.org/10.1111/j.1365-2486.2010.02181.x

Piva, A., Asioli, A., Trincardi, F., Schneider, R.R. and Vigliotti, L. 2008. Late-Holocene climate variability in the Adriatic Sea (Central Mediterranean). *Holocene*, **18**, 153–167, https://doi.org/10.1177/0959683607085606

Powell, E.N., Kuykendall, K.M. and Moreno, P. 2017. The death assemblage as a marker for habitat and an indicator of climate change: Georges Bank, surfclams and ocean quahogs. *Continental Shelf Research*, **142**, 14–31, https://doi.org/10.1016/j.csr.2017.05.008

Prampolini, M., Angeletti, L., Castellan, G., Grande, V., Le Bas, T., Taviani, M. and Foglini, F. 2021. Benthic habitat map of the southern Adriatic Sea (Mediterranean Sea) from object-based image analysis of multi-source acoustic backscatter data. *Remote Sensing*, **13**, 2913, https://doi.org/10.3390/rs13152913

Pratt, N., Chen, T. *et al*. 2019. Temporal distribution and diversity of cold-water corals in the southwest Indian Ocean over the past 25 000 years. *Deep Sea Research Part I: Oceanographic Research Papers*, **149**, 103049, https://doi.org/10.1016/j.dsr.2019.05.009

Ramirez-Llodra, E., Tyler, P.A. *et al*. 2011. Man and the last great wilderness: human impact on the deep sea. *PLoS One*, **6**, e22588, https://doi.org/10.1371/journal.pone.0022588

Reimer, P.J. and McCormac, F.G. 2002. Marine radiocarbon reservoir corrections for the Mediterranean and Aegean Seas. *Radiocarbon*, **44**, 159–166, https://doi.org/10.1017/S0033822200064766

Reimer, P.J. and Reimer, R.W. 2001. A marine reservoir correction database and on-line interface. *Radiocarbon*, **43**, 461–463, https://doi.org/10.1017/S0033822200038339

Reimer, P.J., Bard, E. *et al*. 2013. IntCal13 and Marine13 radiocarbon age calibration curves 0–50 000 years cal BP. *Radiocarbon*, **55**, 1869–1887, https://doi.org/10.2458/azu_js_rc.55.16947

Ridente, D., Foglini, F., Minisini, D., Trincardi, F. and Verdicchio, G. 2007. Shelf-edge erosion, sediment failure and inception of Bari Canyon on the Southwestern Adriatic Margin (Central Mediterranean). *Marine Geology*, **246**, 193–207, https://doi.org/10.1016/j.margeo.2007.01.014

Rillo, M.C., Kucera, M., Ezard, T.H. and Miller, C.G. 2019. Surface sediment samples from early age of seafloor exploration can provide a late nineteenth century baseline of the marine environment. *Frontiers in Marine Science*, **5**, 517, https://doi.org/10.3389/fmars.2018.00517

Ritter, M.D.N., Erthal, F., Kosnik, M., Coimbra, J.C. and Kaufman, D.S. 2017. Spatial variation in the temporal resolution of subtropical shallow-water molluscan death assemblages. *Palaios*, **32**, 572–583, https://doi.org/10.2110/palo.2017.003

R Core Team 2021. *R: a Language and Environment for Statistical Computing*. R Foundation for Statistical Computing, Vienna, Austria, https://www.R-project.org/

Roberts, J.M., Harvey, S.M., Lamont, P.A., Gage, J.D. and Humphery, J.D. 2000. Seabed photography, environmental assessment and evidence for deep-water trawling on the continental margin west of the Hebrides. *Hydrobiologia*, **441**, 173–183, https://doi.org/10.1023/A:1017550612340

Rogers, A.D. 1999. The biology of *Lophelia pertusa* (Linnaeus 1758) and other deep-water reef-forming corals and impacts from human activities. *International Review of Hydrobiology*, **84**, 315–406, https://doi.org/10.1002/iroh.199900032

Romanin, M., Crippa, G. *et al*. 2018. A sampling strategy for recent and fossil brachiopods: selecting the optimal shell segment for geochemical analyses. *Rivista Italiana di Paleontologia e Stratigrafia*, **124**, 343–359, https://doi.org/10.13130/2039-4942/10193

Rosso, A., Vertino, A. *et al*. 2010. Hard-and soft-bottom thanatofacies from the Santa Maria di Leuca deep-water coral province, Mediterranean. *Deep Sea Research Part II: Topical Studies in Oceanography*, **57**, 360–379, https://doi.org/10.1016/j.dsr2.2009.08.024

Sanfilippo, R., Vertino, A., Rosso, A., Beuck, L., Freiwald, A. and Taviani, M. 2013. Serpula aggregates and their role in deep-sea coral communities in the southern Adriatic Sea. *Facies*, **59**, 663–677, https://doi.org/10.1007/s10347-012-0356-7

Schröder-Ritzrau, A., Freiwald, A. and Mangini, A. 2005. U/Th-dating of deep-water corals from the eastern North Atlantic and the western Mediterranean Sea. *In*: Freiwald, A. and Roberts, J.M. (eds) *Cold-Water Corals and Ecosystems*. Springer, Berlin, 157–172.

Siani, G., Paterne, M., Arnold, M., Bard, E., Métivier, B., Tisnerat, N. and Bassinot, F. 2000. Radiocarbon reservoir ages in the Mediterranean Sea and Black Sea. *Radiocarbon*, **42**, 271–280, https://doi.org/10.1017/S0033822200059075

Siani, G., Paterne, M., Michel, E., Sulpizio, R., Sbrana, A., Arnold, M. and Haddad, G. 2001. Mediterranean Sea surface radiocarbon reservoir age changes since the last glacial maximum. *Science (New York, NY)*, **294**, 1917–1920, https://doi.org/10.1126/science.1063649

Siani, G., Magny, M., Paterne, M., Debret, M. and Fontugne, M. 2013. Paleohydrology reconstruction and Holocene climate variability in the South Adriatic Sea. *Climate of the Past*, **9**, 499–515, https://doi.org/10.5194/cp-9-499-2013

Simões, M.G., Rodrigues, S.C. and Kowalewski, M. 2009. Bouchardia rosea, a vanishing brachiopod species of the Brazilian platform: taphonomy, historical ecology and conservation paleobiology. *Historical Biology*, **21**, 123–137, https://doi.org/10.1080/08912960903315559

Sion, L., Calculli, C. *et al*. 2019. Does the Bari Canyon (Central Mediterranean) influence the fish distribution and abundance? *Progress in Oceanography*, **170**, 81–92, https://doi.org/10.1016/j.pocean.2018.10.015

Smith, S.D. 2008. Interpreting molluscan death assemblages on rocky shores: are they representative of the regional fauna? *Journal of Experimental Marine*

Biology and Ecology, **366**, 151–159, https://doi.org/10.1016/j.jembe.2008.07.019

Stefani, M. and Vincenzi, S. 2005. The interplay of eustasy, climate and human activity in the late Quaternary depositional evolution and sedimentary architecture of the Po Delta system. *Marine Geology*, **222**, 19–48, https://doi.org/10.1016/j.margeo.2005.06.029

Sturany, R. 1896. Zoologische Ergebnisse. VIII. Brachiopoden, gesammelt auf den Expeditionen SM Schiffes 'Pola' 1890–1894. *Denkschriften der Kaiserliche Akademie der Wissenschaften in Wien*, **63**, 37–38.

Šimunović, A. 1997. Quantitative and qualitative investigations of benthic communities in the areas of mobile bottoms of the Adriatic Sea. *Acta Adriatica*, **38**, 77–194.

Taviani, M. 1978. Associazioni a Molluschi pleistoceniche-attuali dragate nell'Adriatico meridionale. *Italian Journal of Zoology*, **45**, 297–306.

Taviani, M., Angeletti, L. *et al*. 2016. Reprint of 'on and off the beaten track: Megafaunal sessile life and Adriatic cascading processes'. *Marine Geology*, **375**, 146–160, https://doi.org/10.1016/j.margeo.2015.10.003

Taviani, M., Angeletti, L., Foglini, F., Corselli, C., Nasto, I., Pons-Branchu, E. and Montagna, P. 2019. U/Th dating records of cold-water coral colonization in submarine canyons and adjacent sectors of the southern Adriatic Sea since the Last Glacial Maximum. *Progress in Oceanography*, **175**, 300–308, https://doi.org/10.1016/j.pocean.2019.04.011

Tesi, T., Langone, L., Goni, M.A., Turchetto, M., Miserocchi, S. and Boldrin, A. 2008. Source and composition of organic matter in the Bari canyon (Italy): dense water cascading v. particulate export from the upper ocean. *Deep Sea Research Part I: Oceanographic Research Papers*, **55**, 813–831, https://doi.org/10.1016/j.dsr.2008.03.007

Tesi, T., Asioli, A. *et al*. 2017. Large-scale response of the Eastern Mediterranean thermohaline circulation to African monsoon intensification during sapropel S1 formation. *Quaternary Science Reviews*, **159**, 139–154, https://doi.org/10.1016/j.quascirev.2017.01.020

Thayer, C.W. 1977. Recruitment, growth, and mortality of a living articulate brachiopod, with implications for the interpretation of survivorship curves. *Paleobiology*, **3**, 98–109, https://doi.org/10.1017/S0094837300005157

Thiagarajan, N., Gerlach, D. *et al*. 2013. Movement of deep-sea coral populations on climatic timescales. *Paleoceanography*, **28**, 227–236, https://doi.org/10.1002/palo.20023

Tomašových, A. and Kidwell, S.M. 2017. Nineteenth-century collapse of a benthic marine ecosystem on the open continental shelf. *Proceedings of the Royal Society B: Biological Sciences*, **284**, 20170328, https://doi.org/10.1098/rspb.2017.0328

Tomašových, A., Kidwell, S.M., Barber, R.F. and Kaufman, D.S. 2014. Long-term accumulation of carbonate shells reflects a 100-fold drop in loss rate. *Geology*, **42**, 819–822, https://doi.org/10.1130/G35694.1

Tomašových, A., Kidwell, S.M. and Barber, R.F. 2016. Inferring skeletal production from time-averaged assemblages: skeletal loss pulls the timing of production pulses towards the modern period. *Paleobiology*, **42**, 54–76, https://doi.org/10.1017/pab.2015.30

Tomašových, A., Gallmetzer, I., Haselmair, A., Kaufman, D.S., Vidović, J. and Zuschin, M. 2017. Stratigraphic unmixing reveals repeated hypoxia events over the past 500 yr in the northern Adriatic Sea. *Geology*, **45**, 363–366, https://doi.org/10.1130/G38676.1

Tomašových, A., Gallmetzer, I., Haselmair, A., Kaufman, D.S., Mavrič, B. and Zuschin, M. 2019. A decline in molluscan carbonate production driven by the loss of vegetated habitats encoded in the Holocene sedimentary record of the Gulf of Trieste. *Sedimentology*, **66**, 781–807, https://doi.org/10.1111/sed.12516

Trincardi, F., Foglini, F. *et al*. 2007*a*. The impact of cascading currents on the Bari Canyon System, SW-Adriatic margin (Central Mediterranean). *Marine Geology*, **246**, 208–230, https://doi.org/10.1016/j.margeo.2007.01.013

Trincardi, F., Verdicchio, G. and Miserocchi, S. 2007*b*. Seafloor evidence for the interaction between cascading and along-slope bottom water masses. *Journal of Geophysical Research: Earth Surface*, **112**, F03011, https://doi.org/10.1029/2006JF000620

Trincardi, F., Argnani, A. and Correggiari, A. 2011. *Note illustrative della Carta Geologica dei Mari Italiani, alla scala 1: 250 00*. Foglio NK33-6 Vieste, e Foglio NK33-8/9 Bari, 1–194.

Turchetto, M., Boldrin, A., Langone, L., Miserocchi, S., Tesi, T. and Foglini, F. 2007. Particle transport in the Bari canyon (southern Adriatic Sea). *Marine Geology*, **246**, 231–247, https://doi.org/10.1016/j.margeo.2007.02.007

Turley, C.M., Roberts, J.M. and Guinotte, J.M. 2007. Corals in deep-water: will the unseen hand of ocean acidification destroy cold-water ecosystems? *Coral Reefs (online)*, **26**, 445–448, https://doi.org/10.1007/s00338-007-0247-5

Tyson, R.V. 2001. Sedimentation rate, dilution, preservation and total organic carbon: some results of a modelling study. *Organic Geochemistry*, **32**, 333–339, https://doi.org/10.1016/S0146-6380(00)00161-3

Verdicchio, G., Trincardi, F. and Asioli, A. 2007. Mediterranean bottom-current deposits: an example from the Southwestern Adriatic Margin. *Geological Society, London, Special Publications*, **276**, 199–224, https://doi.org/10.1144/GSL.SP.2007.276.01.10

Vertino, A., Taviani, M. and Corselli, C. 2019. Spatiotemporal distribution of Mediterranean cold-water corals. *In*: Orejas, C. and Jimenez, C. (eds) *Mediterranean Cold-Water Corals: Past, Present and Future*. Springer, Cham, 67–83.

von Allmen, K., Nägler, T.F. *et al*. 2010. Stable isotope profiles (Ca, O, C) through modern brachiopod shells of *T. septentrionalis* and *G. vitreus*: implications for calcium isotope paleo-ocean chemistry. *Chemical Geology*, **269**, 210–219, https://doi.org/10.1016/j.chemgeo.2009.09.019

Walter, L.M., Bischof, S.A., Patterson, W.P. and Lyons, T.W. 1993. Dissolution and recrystallization in modern shelf carbonates: evidence from pore water and solid phase chemistry. *Philosophical Transactions of the Royal Society of London Series A: Physical and Engineering Sciences*, **344**, 27–36, https://doi.org/10.1098/rsta.1993.0072

Warwick, R.M. and Turk, S.M. 2002. Predicting climate change effects on marine biodiversity: comparison of

recent and fossil molluscan death assemblages. *Journal of the Marine Biological Association of the United Kingdom*, **82**, 847–850, https://doi.org/10.1017/S0025315402006227

Weber, K. and Zuschin, M. 2013. Delta-associated molluscan life and death assemblages in the northern Adriatic Sea: implications for paleoecology, regional diversity and conservation. *Palaeogeography, Palaeoclimatology, Palaeoecology*, **370**, 77–91, https://doi.org/10.1016/j.palaeo.2012.11.021

Yasuhara, M., Cronin, T.M., Demenocal, P.B., Okahashi, H. and Linsley, B.K. 2008. Abrupt climate change and collapse of deep-sea ecosystems. *Proceedings of the National Academy of Sciences*, **105**, 1556–1560, https://doi.org/10.1073/pnas.0705486105

Zuschin, M. and Oliver, P.G. 2005. Diversity patterns of bivalves in a coral dominated shallow-water bay in the northern Red Sea – high species richness on a local scale. *Marine Biology Research*, **1**, 396–410, https://doi.org/10.1080/17451000500456262